PART I

DEPENDENCE OF STRESS RUPTURE AND SUPERPLASTICITY ON STRUCTURE IN Co-W ALLOYS

by

C. Vishnevsky and J. F. Wallace*

*Graduate Assistant and Professor of Metallurgy, Metallurgy Department, Case Western Reserve University.

ABSTRACT

Stress rupture tests of four Co-W base alloys were conducted at 1800 and 1850°F in air using as cast specimens produced in conventional investment molds and unidirectionally solidified. These alloys were also extruded to investigate the properties of hot worked structures. Variable strain rate tests of extruded Co-45W-0.05Zr at 1800°F were employed in a study of superplasticity.

In as cast alloys, changes inrupture life and ductility on unidirectional solidification were determined by the favorable longitudinal alignment of grain boundaries competing with the geometry, orientation, and distribution of second phases. For all but modified Co-45W (wt. %), ductility was increased. Rupture life after unidirectional solidification was higher for Co-35W but lower for modified Co-35W. In Co-45W-0.05Zr and modified Co-45W, rupture life was greater for the unidirectional structure at low stresses only. Extruded Co-35W-0.05Zr and Co-45W-0.05Zr experienced a nearly 100 fold degradation in rupture life but large increase in ductility.

The existence of superplasticity in extruded Co-45W-0.05Zr was established. The necessity of a fine structure for

superplasticity was demonstrated; the role of phase transformation was secondary. Continued recrystallization or grain boundary migration during deformation was suggested by microstructural evidence.

INTRODUCTION

As cast structure control is receiving increasing attention and stature as a means of optimizing alloy properties. The influence of cast structure is not limited to applications requiring no subsequent mechanical working. Indeed, it may affect both the actual working process and later material performance.

Two general areas of activity characterizing cast structure research are (1) structure refinement and (2) controlled solidification. Structure refinement deals with the size reduction of individual units such as grains, dendrites, segregates or inclusions. The aim here is to minimize segregation, achieve uniformity and isotropy and derive any possible strengthening effect of fine grained or disperse microstructures. Rapid cooling, small alloying additions, and mechanical techniques such as vibration of the melt have been utilized.

The most convenient and widely studied method is alloying. In "eutectic modification" small additions of various elements are used to alter substantially the usual eutectic morphology producing a finer structure with improved properties. In A1–Si alloys, historically the first of the modified eutectics,

small additions of Na (<. 05%) or certain other elements under usual cooling conditions or only rapid solidification produce modification. The list also includes ductile iron made by treating gray iron with small amounts of Ce or Mg, and more recently, a number of high temperature eutectics, Co-W, Co-Al, Ni-W, Ni-Ta (1).

Refinement of as cast structures by alloying in non-eutectic systems has found widespread application. Alloys of aluminum (2), magnesium (3), copper (4), steels (5) and a number of high temperature alloys (6) are among the many examples of successful applications of refinement.

An understanding of the above phenomena and their effects on mechanical properties is related intimately to knowledge of solidification. As such the complex multi-element interactions affecting the nucleation and growth phenomena influencing these structures will not be reviewed now.

The second broad area of cast structure research deals with controlled solidification. Here control of the microstructure results from external thermal control of the solidification process. In its most sophisticated form both the thermal gradient and solidification rate are regulated. The technique has certain obvious merits. Efficient feeding of the casting is enhanced,

reducing porosity and the dendritic structure is more uniform. But the greatest benefit is the development of structural anisotropy which, properly utilized, is desirable in certain applications.

Controlled or unidirectional solidification generally produces two distinct effects, regular or preferred alignment of microconstituents and preferred grain and grain boundary orientation. In the field of fiber reinforced metal matrix composites the potential of structures with reinforcing fibers produced in situ is most attractive. It has been demonstrated that controlled eutectics with rod or lamellar structures, aligned in the direction of solidification and subsequent loading, can exhibit fiber reinforcement (7, 8). The choice of matrix and reinforcing phases, the morphology, whether rod, lamellar or anomalous, and volume fraction of reinforcing phase are obviously limited by existing eutectic systems. Comparatively few binary systems have been studied. Many of these are promising (9). Furthermore, when one considers higher order systems, the field is virtually untapped. Most of the work to date has dealt with room temperature properties, although elevated temperature reinforcement is also being investigated. Here even more progress remains to be realized, with high temperatures introducing

complications. Thus, Ta_2C fibers in a Ta matrix led to reinforcement at room temperature, but a rapid decrease in strength at elevated temperature (10).

In controlled eutectics where fiber reinforcement is sought, the dominant strengthening mechanism is load transfer from matrix to fiber. Particularly at lower temperatures grain and grain boundary alignment is likely to be of secondary importance. However, in other than eutectic systems and indeed in certain eutectics, unidirectional solidification does not produce proper second phase alignment for reinforcement in the direction of solidification. Structural anisitropy in such ,alloys leads to mechanical property effects substantially different in nature from those found in composites. In some recent work on high strength steels alignment of sulfides along dendrite arms produced marked differences in transverse and longitudinal properties (11).

Unfavorable distributions of second phases resulting from unidirectional solidification were also observed in a high temperature, high carbon austenitic steel and high carbon Stellite alloy *(6)*. Failures initiated at carbides aligned perpendicular to the solidification direction. Control of equiaxed grain size was utilized to improve the carbide morphology and enhance creep strength and ductility.

An analysis of structural effects in controlled solidification must also include consideration of grain and grain boundary effects. At low temperatures, a small grain size is desirable with grain boundaries being stronger than the grains. At high temperatures, past the so-called equicohesive temperature (12) a transition occurs where the boundary strength falls below that of the grains. Furthermore, creep failures often propagate intergranularly with voids preferentially initiating on boundaries perpendicular to the tensile loading direction.

It has been shown that controlled cast structures can reduce these causes of elevated temperature weakness. Unidirectional solidification of a Ni-Cr-Al superalloy, in which the strengthening is derived from a fine dispersion of γ' Ni_3Al intermetallic, aligned the grain boundaries longitudinally (13). This led to improvements in both stress rupture life and ductility over equiaxed or transverse columnar structures. More recently the techniques of unidirectional solidification have been applied commercially to the production of jet turbine blades. Both stress rupture life and elevated temperature ductility were increased over conventional investment cast blades (14, 15). The full potential of this alloy was not realized by unidirectional solidification, in which numerous grains are aligned longitudinally,

because of the persistence of a few transverse boundaries.

Single crystal blades have also been successfully cast and the stress rupture life, ductility, and minimum creep rate improved compared to unidirectionally solidified multi-grain columnar structures **(14,** 15). This latter development represents a significant advance in the attainment of optimum properties through cast structure control. However, as noted earlier, factors other than grain boundary orientation may be influential. In addition to second phase distribution and orientation, crystalline anisotropy, changes in flow properties and modulus, are no doubt important.

The present study was undertaken to provide additional insight into the influences of microstructure at elevated temperatures. Specifically, the purpose of this investigation was two-fold: first, to analyze the role of grain boundary and second phase orientation on the stress rupture behavior of as cast Co-W base alloys and secondly, to examine the effects of controlled cast structures on the extrusion and subsequent creep strength of these alloys.

MATERIALS AND PROCEDURE

Alloys Investigated

Based on earlier work (16) two pairs of alloys, Co-35W and co-45W base, were selected for the present study. The choice of these alloys resulted from the large differences in properties and particularly structures exhibited by as cast stress rupture specimens. The nominal compositions in weight percent of the Co-35W base alloys were Co-35W-0.05Zr and Co-35W, 3Cr, 2Ti, 2Zr, 1C, 0.1B. The slight amount of Zr was added to the former alloy for deoxidation and was not sufficient to modify the structure of that binary composition. The second, modified Co-35W, alloy was also developed by Ramseyer **(16)** and possesses excellent 1850°F stress rupture properties. The possibility of further improvement by unidirectional solidification was thought to be worth pursuing.

The second pair of alloys was based on the Co-45W eutectic composition. **AS** with the 35W base alloy, one of these was unmodified containing Co-45W-0.05Zr. Modification of the eutectic with 0.75Ti, 0.75Zr, 0.25C, 0.1B has been shown to improve stress rupture behavior markedly (16). This latter alloy was also included in the current work.

Melting Materials and Chemical Analysis

High purity elemental materials were melted to obtain the desired alloys. Their purity and form were as follows:

Element	Form	Purity
Co	electrolytic, 1 x 1 x 1/8"	99.5+
W	powder, 6 micron avg.	99.9+
Cr	electrolytic	99.8+
Ti	sponge	99.65
Zr	sponge (reactor grade)	99.8+
C	spectroscopic graphite	99.999+
B	-325 mesh	99.25

Both wet chemical and X-ray fluorescent analyses were performed by an outside laboratory. Once the melting techniques were established, excellent reproducibility of compositions was obtained and analyses were not conducted for all elements of each heat.

Melting Practice

Heats weighing approximately 4-5 pounds were induction melted in stabilized ZrO_2 crucibles surrounded by a graphite susceptor. A new crucible was used for each heat. The 250 KW

induction unit operated at 960 cps. The melting furnace, auxiliary mold heater, and molds were located in a chamber which could either be evacuated or filled with a protective atmosphere.

The entire charge could not be placed in the crucible. Accordingly, all of the W, C, B, and Cr together with most of the Co were packed initially. Once this charge had melted the remaining Co was added remotely via a charging chute, Ti and Zr additions were made shortly before pouring the metal.

Two melting procedures were employed. For the unmodified alloys, the initial charge was gradually heated to incipient melting, the chamber filled to 1/2 atmosphere of argon, and the rest of the Co added. Once the entire charge was molten, it was permitted to cool under reduced power until a thin solid skin formed and then heated gradually to incipient melting. At this time, the melting point was established with an optical pyrometer. The bath temperature was then raised to 100°F (optical) above the melting point and the chamber evacuated to a pressure of 150 μ Hg over a 15 minute period. The purpose of this pressure reduction or boil was to lower the gas content in the melt. After the boil, the chamber was backfilled with argon to a pressure of 5/6 atmosphere. The temperature was then raised to 350°F (optical) above the melting point, the Zr

was added, and the metal poured into a preheated mold.

The modified **Co-35W** and **Co-45W** base alloys contained carbon and required a slightly different melting procedure. During the boil the chamber pressure was lowered very slowly to prevent vigorous sputtering and ejection of molten droplets. The boiling period was twenty minutes; the pressure was lowered to only 1/6 atmosphere of argon. The final alloy addition before pouring contained both Ti and Zr. Otherwise the melting and pouring practice did not differ from that used for the unmodified alloys.

The metal temperature changes above the melting point as measured with the optical pyrometer was less than the actual differences determined by a Pt, Pt - 10% Rh immersion thermocouple. Superheats of 100° and 350°F (optical) corresponded approximately to actual changes of 125' and 500°F.

Molds and Auxilliary Equipment

Four different ceramic shell molds were used to produce test material. These molds and typical castings are illustrated in Figures 1 and **2.** The molds contained a dip coat of zircon and were made by the lost wax process. Conventionally cast test bars were poured in the form of clusters,

Figure 1(a). The mold was preheated to 1600°F in an electric resistance furnace. Immediately after pouring the mold furnace power was shut off and the casting permitted to cool gradually to room temperature. The test specimens were then cut off from the ingates and sandblasted lightly to remove any light scale and reveal possible surface imperfections,

Unidirectionally solidified castings were poured into a modified version of the conventional cluster mold, Figure 1(b). The lower portion of this mold was cut off to permit heat extraction by a water cooled copper chill. The mold and chill block were located in a 4 KW electric resistance heated (SiC Globar element) furnace capable of operating at 2500°F in vacuo and 2800°F in argon. The furnace is illustrated in Figure 3. This furnace was also used for preheating the conventional cluster molds.

Unidirectional solidification was obtained by pouring metal from the induction furnace into the heated mold. The sides of the mold were maintained above the liquidus. For cluster molds, this temperature was 2780°F. Furnace power was not reduced until ten minutes after pouring. The structure of as cast test bars was unidirectional over most of the specimen length, including the entire test section. The dendrite

spacing in the reduced center section was fairly constant.

In addition to as cast test bars, ingots for subsequent extrusion were also cast. Unidirectionally solidified castings were produced in the ceramic mold shown in Figure 2(b) using the previously described mold furnace. A mold temperature ranging from 2650°F to 2750°F was required to obtain unidirectional structures with no surface nucleation. The columnar zone length in all cases was over 2 3/4". For conventionally cast ingots the mold (Figure 2(a)) was supported in silica sand bonded with 1% sodium silicate. This arrangement was preheated in a gas fired furnace to 400°F and placed into the vacuum chamber immediately before the start of a heat. After pouring, a granulated exothermic hot topping compound was added to the top of the casting as soon as a thin solid skin had formed. This provided for more efficient feeding while reducing the possibility of entrapping foreign exothermic material in the ingot,

Extrusion of Cast Ingots

Extrusion billets were machined from conventionally cast and unidirectionally solidified ingots of all four alloys. These were then canned in mild steel. Billet and can dimensions

are shown in Figure 4(a). The extrusions were conducted on a 750 ton capacity horizontal hydraulic press. The die had an included angle of 120' and an orifice diameter of ,750 inches, giving an 8:1 reduction on the total canned assembly. The reduction on the billet was not constant. The reduction on 1 to 2 inches of the extreme nose and tail portions of the extruded billet was between 4: 1 and 6: 1; the rest of the extruded product, from which test specimens were taken, experienced between a 7: 1 and 9: 1 reduction in area. The extrusion lubricant was Cr_2O_3 and graphite grease. Ram speeds ranged from 1 to 4.8 inches per second. Billets were preheated in an argon atmosphere to 2125' -2200°F, depending on the alloy. After extrusion, the bars were cooled on a sand bed. Quantitative data obtained during extrusion consisted of traces showing the variations of ram pressure and speed with time.

Mechanical Testing

Constant load stress rupture tests were performed on as cast bars and specimens machined from sound extrusions, Figure 4(b). All alloys, with the exception of modified Co-35W, were tested at 1800°F; the latter was tested at 1850°F. Stress rupture life, ductility, and, whenever possible, minimum creep

rate were determined. The creep strain was measured by dial gages attached to the weight pan ends of the stress rupture machine loading arms. Specimen slippage in the grips during seating probably introduced some error initially. Except for these early inaccurracies, the curves of creep strain versus time from which minimum creep rates were extracted are considered reliable,

Metallography

Metallographic examination was performed on all cast, extruded, and tested material. Microstructures were revealed by etching mechanically polished specimens with the etchants listed in Table I. Stains produced by some of these etchants were removed by a concentrated aqueous solution of KOH.

The phases observed were identified only by metallographic means. In the unmodified alloys, the phase diagrams of Hansen and Anderko (17) and the recent study of Neumeir and Holman (18) were assumed to apply. The phase diagram of the Co-W system incorporating this latter work appears in Figure 5. Some other investigations (19, 20) were of value in identifying microconstituents in the modified alloys.

RESULTS AND DISCUSSION

Chemical Analysis

The results of chemical analyses on representative heats appear in Table 11. Although W was not analyzed, the actual analysis deduced from sums of other elements determined was approximately 1% less than the nominal value. This coincides with losses reported by Ramseyer (19). The Co contents were correspondingly about 1% above the nominal. The quantity of other elements closely approximated the nominal compositions. The amount of Zr added to the nominal .05 Zr heats was .06%. The recovery was generally very low, indicating that most of the Zr was consumed in deoxidation. In general, with the exception of the .05 Zr heats, the amount of extra material added to obtain desired recoveries was 12% for Ti and Zr, 20% for C and B, and 3% for Cr.

As Cast Alloys

Microstructural Considerations

The microstructures for all alloys investigated appear in Figures 6 to 9. Conventionally cast material in most cases had the same structures as observed in earlier studies (1, 19). Figure 6(a) shows the structure of conventional Co-35W-0.05Zr.

Although the microstructure was not modified appreciably by the addition of this small quantity of Zr, its etching characteristics were altered. The interdendritic precipitate is Widmanstatten Co_3W with some ε possibly present.

Figure 6(b) shows longitudinal sections of this alloy solidified unidirectionally. The precipitate is now better delineated and lies in the interdendritic spaces, parallel to the direction of solidification. Regions of a grain boundary precipitate were also discernable, This precipitate is probably the eutectic formed from segregation of W at the boundaries. Strong support for this contention was found in tested specimens and will be discussed later. The light relatively precipitate free regions in both as cast Co-35W-0.05Zr microstructures are face centered cubic α Co.

The structure of conventionally cast Co-35W, 3Cr, 2Ti, 2Zr, 1C, 0.1B, is shown in Figures 7(a), (b). Ramseyer (19) developed this alloy through systematic additions of Ti, Zr, C showing that the ratio of (Ti+ Zr)/C has a large effect on structures and properties. From the changes in structure and volume fraction of second phases, he deduced that both M_6C and MC were present. X-ray phase identification of electrolytically extracted carbides in a structurally equivalent alloy

with 1Ti, 1Zr, 0.056 showed the presence of M_6C as Co_3W_3C and MC as TiC with probable substitution of Zr (19). Based on the above study, the large idiomorphic particles in Figure 7(a), (b) are believed to be MC carbides; the smaller equiaxed particles and islands of carbide eutectic are probably M_6C carbides.

Unidirectional solidification of this alloy produced the large microstructural changes shown in Figures 7(c), (d). The general structure exhibited a coarse carbide eutectic. Near the mold wall-casting interface, large clusters of faceted MC carbides were present. The eutectic is tentatively identified as M_6C carbide probably arising from local deviations in the proper ratio of Ti+ Zr/C. Very similar structures occurred in Co-35W, 3Cr, 0. 1B base alloys with additions of 0. 5C; 1C; 2Zr + 0.5C; 2Zr + 1C; 2Ti + 1C (19).

Chemical analyses taken at various locations in unidirectionally solidified castings showed no segregation of Ti, Zr or C along the length with some segregation of Ti to the mold wall. The reason for this behavior appears to be the depletion of MC carbidesfrom the central portions of the test section. It is proposed that the MC carbides segregated from the melt to the mold wall in the following manner. The general shape of the liquid-solid interface in a unidirectionally freezing casting

will not be flat in castings solidified by the technique employed in this study. The mold wall temperature must be higher than along the rest of the front to prevent surface nucleation. Under these conditions, it is expected that a roughly dome shaped interface whose crest protudes into the liquid will be obtained. MC carbides, being stable in the liquid, can slough off the interface into the trough formed by the mold and solidifying front.

Figure 8(a) shows the microstructure of conventionally cast Co-45W-0.05Zr. The as cast structure is essentially two phase composed of lamellae of W_6Co_7 or μ phase in FCC α Co. The primary Co is the continuous phase. W_6Co_7 has a rhombohedral structure and can exist over a range of compositions (17, 18). Cast conventionally the lamellae appear in feather-like patterns with main rib of W_6Co_7 and branches of W_6Co_7 and primary Co nearly perpendicular to the ribs. Unidirectional solidification preserved the feather or tree-like pattern, Figure 8(b). The main, relatively coarse, ribs of W_6Co_7 are parallel to the growth direction with branches of W_6Co_7 and primary Co almost perpendicular to it. This type of eutectic growth has been observed in both metal and organic systems and is characteristic of so-called complex-regular binary

eutectics in which one phase has a high while the other has a low entropy of melting (21).

Modification of the Co-45W eutectic with 0.75Ti, 0.75 Zr, 0.25C, 0.1B resulted in a coarser structure. The conventionally cast material, Figure 9(a), contains thick platelets of a η phase W_3Co_3C (20) and small well dispersed carbides, probably MC. The complex-regular eutectic pattern is maintained although the constituents are less acicular. Unidirectional solidification coarsened the structure even further. Large lamellae of the intermetallic are aligned, similar to the Co-45W-0.05Zr alloy, nearly perpendicular to the growth direction while main dendrite ribs are parallel to it, Figure 9(b). The structure illustrated in Figure 9(b) is from a stress rupture specimen tested at 1800°F and shows a matrix precipitate that appears to be Co_3W.

In both of the Co-45W base alloys that were solidified unidirectionally, grain or cell boundaries were aligned parallel to the specimen axis.

Relation of Structure to Properties

The results of all stress rupture tests on as cast specimens are listed in Table III. The changes in rupture life,

creep rate, and ductility varied for the four alloys in the unidirectionally solidified condition. A complete analysis of the results must necessarily consider the structural factors affecting creep resistance, initiation and propagation of failure.

It has been observed for a number of metals and alloys that rupture life and minimum creep rate are inversely related (22, 23) such that in a log-log plot a slope of approximately -1 is obtained. Similar behavior was found in the present study. Figure 10 summarizes all the data obtained in this investigation in one plot. A line with a slope of -1 is drawn through the points. Since a number of variables are combined in this plot, the data actually represent a family of lines, the slope of each is roughly unity. Monkman and Grant (23) concluded that the relation log $t_r + m \log(mcr) = c$, (where t_r is the rupture life, m is the slope, mcr is the minimum creep rate, and c is a constant), is fairly independent of temperature, stress, composition, heat treatment or hardness for a particular alloy system. However, the data obtained in the current investigation are not sufficiently extensive to permit similar conclusions. The implications of this relationship have been well discussed in the literature. It is sufficient only to note that the minimum creep rate and

rupture life would differ in opposite directions when plotted versus stress and be exact mirror images for m = 1.

Curves of initial stress versus rupture life for the Co-35W-0.05Zr alloy appear in Figure 11. Unidirectional solidification produced a two to three fold increase in rupture life over the entire stress range. The superior rupture life of the unidirectional Co-35W-0.05Zr is reflected in a lower minimum creep rate at all stresses, Figure 11. The average ductility of the unidirectional alloy as measured by percent elongation was 13.5% compared to 11.2% for the conventional castings. Average values were used in such comparisons for all alloys since no consistent variation of ductility with stress was evident, although it is often observed that elongation decreases with stress and increasing rupture life **(24).**

Microstructural examination of specimens tested both at high and low stresses showed no perceptible effect of stress level on mode of failure. All specimens contained precipitation of ε and Co_3W in the grains and lamellar eutectic in the grain boundaries, Figure 12, The eutectic was most pronounced in the unidirectional casting and is attributed to gravity segregation of W in the grooves formed by two adjacent grains and the melt. W enrichment in this area would depress the freezing point,

retarding solidification relative to the adjacent grains and further accentuating the grooving. A coarse intergranular precipitate was also present in the conventional castings.

In the latter structure grain boundary sliding was clearly evident, Figure 12(a). Small fairly equiaxed cavities were visible along the sliding boundaries inclined to the testing direction with wedge or W type voids appearing at boundaries nearly perpendicular to it. Figure 12(a) shows decohesion produced by grain boundary sliding. W-type voids are usually associated with grain boundary junctions, triple points, at which sliding is not accommodated (25). They usually grow along the boundaries. A few, very small, rounded voids were also present in the grains. Some were associated with small isolated areas of eutectic and appeared to be stable. Thus, the failure of the conventionally solidified Co-35W-0.05Zr alloy appears to have been initiated intergranularly.

In unidirectionally solidified Co-35W-0.05Zr, the grain boundaries were also the source of weakness. Voids formed at the grain boundary eutectic. Both small rounded and angular cavities were observed, Figure 12(b), but these did not extend into the grains. There were a few small cavities away from the fracture. However, near the fracture surfaces, the boundaries contained continuous or semi-continuous longitudinal fissures. The grains contained a

few rounded voids. Failure in the unidirectional castings apparently was initiated intergranularly at the eutectic precipitate and progressed transgranularly.

The superiority of the unidirectional structure in this alloy, in spite of the heavy grain boundary precipitation, probably resulted from the absence of oblique boundaries and grain boundary sliding. In the conventional casting, decohesion from sliding created large cracks, decreased the load supporting area and increased the stress. This would greatly accelerate further sliding and eventual rupture. In the unidirectionally solidified specimens, grain boundary sliding in the usual sense was absent and voids did not extend transgranularly over large distances.

The stress rupture behavior of the modified Co-35W alloy was not improved by unidirectional solidification. The rupture life was reduced and the minimum creep rate was higher at all testing stresses, as shown in Figure 13. These results are readily interpreted on the basis of structure. Conventionally cast modified Co-35W was very homogeneous. No grain boundary precipitates or other segregation were visible optically. In broken specimens voids appeared at carbides, Figure 14(a). Considerable grain boundary sliding was also evident, Figure 14(b). Much of the strength of this structure can be attributed to the fine and

uniform dispersion of carbides (19).

When this alloy was solidified unidirectionally, the structure was altered appreciably, as discussed earlier. The decrement in creep resistance is attributed at least partially to the clustering of MC carbides at the specimen surface. Many small voids and transverse cracks were present at these clusters in tested specimens. It is highly probable that they started early failure. Figure 14(c) shows cracks emanating from these areas, a condition prevalent both near and far away from the fracture surface.

The behavior of the Co-45W base alloys was more complex. The rupture life of the unidirectionally solidified modified alloy was improved at low stresses but decreased at high stresses, Figure 15. The minimum creep rate exhibitsa similar cross over. At high stresses the creep rate is lower for the conventional structure. Two straight line portions may provide the best description of the rupture life curve.

In the conventional specimens, voids resulted from intermetallic rupture and grain boundary sliding. The many small voids in the grains were usually not extended, indicating some arrest and strengthening from the relatively random arrangement of intermetallic, Figure 16. No variation in void appearance

with stress was noted.

For unidirectional castings, the lamellae were coarser and aligned nearly transversely. The appearance and number of voids varied with stress. In particular, at 20,000 psi many cracks through the intermetallic were observed. These were present both near and away from the fracture surface. No cracks were evident at the intermetallic-matrix interface since at this high stress, the intermetallic was clearly weaker than the matrix or interface. At 17,500 psi the intermetallic contained very few cracks; these were more frequent near the fracture. At even lower stresses of 15,000 and 12,500 psi, fissures were also located at the intermetallic-matrix interface. With the exception of the region immediately adjacent to the fracture, intermetallic cracking was not observed. Figure 17 shows typical cracks found in tested specimens.

The superior creep resistance at low stresses of the unidirectional specimens over the conventional structures is attributed to the favorable, longitudinal alignment of grain boundaries and good cohesion between matrix and intermetallic. At 17,500 and 20,000 psi the unfavorable second phase orientation predominated. The lower ductility of the unidirectional castings reflects the coarse and transverse plate-like structure with its

lack of obstacles to crack extension. A crack could grow unhindered over large distances and decrease greatly the load supporting area, thereby leading to relatively brittle, catastrophic failure, In the conventionally cast material, crack arresting occurred and much larger elongations, nearly four fold, were obtained.

The effect of stress on rupture life and minimum creep rate for Co-45W-0.05Zr is shown in Figure 18. At high stresses the unidirectional structure exhibited lower stress rupture lives and higher creep rates. The stress life curves show a tendency for improved life over conventionally cast material, with decreasing stress for the unidirectional specimens. Correspondingly, the minimum creep rate decreases more rapidly with stress for this latter structure, Microstructural examination did not reveal a variation of fracture mode with stress for either structure.

In conventionally cast specimens, cracks originated at grain junctions. Figure 19(a) shows voids produced by the relative displacement of adjacent grains. In the unidirectionally solidified alloy, voids formed parallel to the nearly transverse lamellae of W_6Co_7 and precipitate, Figure 19(b), and at a few imperfections in the cast structure, Figure 19(c). Generally, these imperfections 'were grains that had nucleated independently.

In contrast with the modified Co-45W alloy, unidirectional

solidification of Co-45W-0.05Zr provided improved creep elongation over conventional castings, 12.3 vs 6.9%. The transverse voids in Co-45W-0.05Zr were much smaller than in modified Co-45W, reflecting the much finer structure of the former alloy. Thus, individual cracks extended over small distances and did not lead to early brittle failure.

However, Co-45W-0.05Zr cannot be regarded merely as a scaled down version of the modified alloy. The intermetallic phases are not the same nor is their stability similar. At the test temperature of 1800°F, the transformation of W_6Co_7 with α to form Co_3W and ϵ (or α) proceeds rapidly. Even at the shorter testing times, heavy precipitation was observed and many smaller particles of W_6Co_7 were dissolved. On the other hand, in modified Co-45W matrix precipitation occurred very slowly and the W_3Co_3C did not appear to be dissolving even after 82+ hours at 1800°, Figure 17(b).

Extruded Alloys

Extrusion billets were machined from both conventionally cast and unidirectionally solidified ingots of all four alloys. The macrostructures of as cast ingots are shown in Figures 20 and 21. Conventionally cast s'tructures were composed largely of trans-

verse columnar grains with a small central equiaxed region. In some ingots this region was virtually nonexistent, During unidirectional solidification the columnar grains were aligned in the direction of solidification with the second phases distributed and aligned in the same manner as previously described for the test specimen castings. The structure near the chill was very fine; the structure was fairly uniform along the length of the central portion; the top of the ingot had a coarse structure. The columnar zone length exceeded 2 **3/4** inches for all ingots or nearly the entire length of **3** inches for the billet.

Workability

Although the primary purpose of extrusion was to examine the effects of subsequent structures on properties, information on hot workability of these alloys was also obtained.

The choice of extrusion for hot working as opposed to forging, rolling or swaging was based on some limited hot upset tests, which indicated that these alloys would be difficult to work. Extrusion is particularly suited to the working of otherwise unmanageable materials since the working stresses are compressive. Within the obvious limitations of available ram pressure, large reductions increase the hydrostatic component

of stress in the deformation zone and aid in obtaining a sound-product. Pugh and Gunn (26), in varying both back pressure and reduction in hydrostatic extrusion, demonstrated the efficacy of sufficiently large reductions in reducing or even eliminating the counterpressure required to prevent cracking in magnesium.

In the present study, an 8:1 reduction was the largest reduction that would still yield a sufficiently large product for testing. A number of parameters were evaluated during the course of each extrusion to obtain an indication of the ease with which the material was deformed. For a particular set of conditions (material, die, lubrication, temperature, and deformation rate) the variation of ram pressure with ram travel was measured. A schematic representation of such a pressure travel record appears in Figure 22(a). An initial pressure peak arises from the frictional forces between a long, undeformed billet and the press container and die and initial deformation in the die. Once material is being forced through the die, the length of undeformed billet decreases, reducing billet-container friction and the heat produced by deformation contributes to lowering the strength of the billet, particularly at high temperatures and strain rates. With low billet container friction, this latter portion of a curve ("run pressure") tends to be flat. A typical pressure trace simultaneously

showing ram speed appears in Figure 22(b).

The data obtained from extruding ten billets are listed in Table IV. For all billets very sharp peak pressures were observed with the run pressures being fairly constant. The peak pressures were generally high, approaching the maximum allowable ram pressure of 177,000 psi,

The quality of the various extrusions differed appreciably. Even in the as extruded condition, a cursory visual inspection indicated that some of the extrusions were unsatisfactory. The pieces illustrated in Figure 23(a) appeared to be sound, whereas those shown in Figure 23(b) consisted of small chunks either in loose form or still encased in the steel jackets. These latter bars were produced from the modified Co-45W alloy.

Various combinations of extrusion conditions were employed in attempts to obtain sound material for this alloy, At a speed of 6 inches per second and 2200°F the extrusion of a conventionally cast ingot resulted in a poor product, Figure 23(b), #1. At 2150°F and a slower speed of 1.8 incher per second another conventional ingot was not extruded successfully, Figure 23(b), #2. An attempt was then made to extrude a unidirectionally solidified ingot at 2100°F, but it stalled,in the die without upsetting. The can was remachined and the piece extruded through an .885 inch diameter

die at a somewhat higher temperature of 2125°F. Again the product was unsatisfactory, Figure 23(b), #3. It was concluded that modified Co-45W probably cannot be hot worked. The coarse lamellar structure of this alloy, which must be broken up considerably to achieve smooth metal flow during deformation, is considered to be responsible for the inadequate workability.

Radiographic examination of the remaining extrusions revealed fine internal tears in the modified Co-35W alloy. These tears were located along most of the unidirectionally solidified extrusion. The conventionally cast ingot yielded a radiographically sounder product and a number of test specimens were machined from it. In view of the varying condition of the modified Co-35W alloy extrusions, a comparison of working pressures for this alloy was not valid.

The two unmodified Co-35W billets were extruded at somewhat different temperatures. The product was generally satisfactory, although a few isolated regions contained slight tears. Sufficient sound material was available for test specimens from both extruded pieces.

The best extrusions were obtained from Co-45W-0.05Zr ingots. A comparison of extrusions **6** and **7** (Table IV) shows that for the same extrusion speed the unidirectionally solidified structure

required a higher run pressure. In the final product the intermetallic was aligned longitudinally for both billets. In the unidirectionally solidified ingot, the lamellae were aligned nearly perpendicular to their extruded orientation; in the conventionally cast ingot, the initial arrangement was more random and some lamellae did not require much additional realignment. The difference in run pressures probably reflects the extent to which the less ductile phases in the cast structure had to be rearranged into the final longitudinal array. The peak pressures differed in the opposite direction, but these are probably less sensitive to structure and more dependent on the initial speed with which the ram contacts the billet. This speed was high to minimize heat loss to the container.

Extruded Structures and Properties

Figure 24 shows the transverse macrostructural appearance of extruded **Co-35W-0.05Zr.** It is evident that the cast ingot pattern was not eliminated with the nominal 8:1 reduction. This is illustrated further by the microstructures of transverse sections, Figures 25(a), (b). The regular alignment of dendrites within unidirectional grains is preserved on extrusion, Figure 25(b). The longitudinal microstructures, Figures 25(c), (d), differed less.

In both extrusions the grain size is similar and the second phases are aligned longitudinally. The recrystallized grains of α Co contain annealing twins.

The modified Co-35W after extrusion contained voids both at the ends of MC carbides and as small tears, Figure 26. The conversion of globular or eutectic M_6C carbides present in the cast condition into a fine net-like structure indicates overheating during extrusion.

Two types of extruded microstructures, corresponding to cast ingot structures, were obtained for Co-45W-0.05Zr. From both transverse and longitudinal sections, it was established that the W_6Co_7 was aligned longitudinally in the form of sheets. Extrusion of unidirectionally solidified ingots produced a very uniform microstructure with little variation in size of intermetallic particles or matrix grain size, Figure 27 (a),(b). The structure of the extruded conventional ingot was less uniform with banded regions of predominately very fine intermetallic, Figure 27(c), intermixed with areas of coarse intermetallic and larger grains. Figure 27(d) shows such a coarse area. In both types of structures small voids were present at the ends of many intermetallic particles in the longitudinal section. The pointed shape of these voids suggests laminar-like flow of the matrix around the

less ductile particles. At the extrusion temperature of 2200°F the structure was α Co and W_6Co_7. Fairly rapid cooling of the extruded product preserved this structure. The α Co grain size is very fine, on the order of a few microns.

The stress rupture properties of the above three alloys were greatly altered by extrusion. The results of limited stress rupture tests are listed in Table V.

Only one sample of modified Co-35W was tested. It fractured with little ductility almost as soon as the load was applied. Apparently the extruded structure with its voids and continuous precipitate films did not permit a proper evaluation of the stress rupture behavior of this composition.

For the Co-35W-0.05Zr alloy, extrusion decreased the rupture life by nearly a factor of 100, as shown by the stress rupture curves in Figure 28. The ductility, however, was increased. Two samples of a unidirectionally cast and extruded bar had an average elongation of 62.5% compared to 13.5% for the as cast unidirectional alloy. A third specimen, from an extruded conventional ingot, elongation 174% with multiple necks, Figure 29(a).

The variation of rupture life with stress for extruded Co-45W-0.05Zr is given in Figure 30. The decrease in life over

cast material is again nearly hundredfold. The increase in ductility accompanying the strength drop was most remarkable. One sample elongated 212%, the extension limit of the testing machine, without fracture or necking. The deformation was extremely uniform with no indication that stretching capacity was exhausted, Figure 29(b).

A large increase in ductility, rationalized merely the basis of degradation in strength, would not account for the necking resistance. As such, the observed behavior of extruded Co-45W-0.05Zr bears strong resemblance to the phenomenon of superplasticity which is characterized by large amounts of neck-free elongation (27).

Accordingly, a series of experiments was performed using extruded Co-45W-0.05Zr in an effort to establish more conclusively the existence of superplasticity in this alloy and examine the mechanisms involved. These experiments and their results are described in the following section.

CONSIDERATIONS OF SUPERPLASTICITY

As applied to metals, superplasticity is a relatively recently observed phenomenon characterized by unusually large ductility before fracture. Elongations of nearly 2,000% have been reported (28). The common behavior of ductile metals under tensile loading is to fail shortly after the onset of plastic instability or necking. Superplastic metals, however, exhibit viscous-like behavior, low strength and necking resistance. Thus, the appearance of stretched, broken specimens is more reminiscent of drawn glass than the common cup-cone fracture of ductile metals. Superplasticity is not peculiar to tensile tests, although most of the attention has been devoted to this type of loading. **A** review by Underwood (29) summarized much of the work on the subject prior to 1962.

Some ambiguity exists regarding the sorts of effects that should be labelled superplastic. Nevertheless, most of these can be classified into either transformation plasticity produced by deformation during a phase change with thermal cycling during the test or the more conventional superplasticity in which the test temperature is constant.

Considerable attention has been given to superplasticity

in binary eutectics, notably Al-Cu, and eutectoid Al-Zn by Soviet researchers **(29).** In as cast specimens, superplasticity occurred only in metastable structures produced by quenching from a single phase field and testing in the **two** phase region near the transformation temperature. Homogenized material did not show superplasticity. The general Soviet view has favored metastability as a necessary condition for superplasticity. In quenched alloys of certain systems, compositional equilibrium restored by diffusion and deformation is believed to cause the abnormal ductility.

More recent work indicates that metastability per se is not a prerequisite for superplasticity. Petty (30) obtained superplasticity in several extruded and subsequently annealed Cu-A1 alloys. This behavior was, in part, attributed to the ability of $CuAl_2$ particles to interfere with crack propagation.

Backofen and his co-workers have demonstrated in Al-Cu (31) and Pb-Sn (32) eutectics that a fine structure characterized by a grain size of few microns is an alternative way of obtaining superplasticity. They have analyzed necking resistance in terms of strain rate sensitivity using the relationship $\sigma = K \dot{\varepsilon}^m$ (27, 31, 32) (where σ = stress, K = a constant, $\dot{\varepsilon}$ = strain rate, m = strain rate sensitivity index).

When the strain rate sensitivity index, m, is unity, the equation describes purely viscous flow. For metals at elevated temperatures, m seldom reaches 0.3; usual high values are in the range of 0. 1 (33). It has been demonstrated that necking resistance increases with m **(27).** Thus, combining $\sigma = K\dot{\varepsilon}^{m} = F/A$ (where F = force and A = cross sectional area) with

$$\dot{\varepsilon} = -\frac{1}{A}\frac{dA}{dt}$$

yields

$$-\frac{dA}{dt} = \left[\frac{F}{K}\right]^{1/m}\left[\frac{1}{A^{\frac{1-m}{m}}}\right]$$

For m = 1, the rate of change in area at any point is not a function of the area and necks or other discontinuities such as cracks are stable in deformation. To date, values of m as high as **0.75** have been reported in superplastic metals (31).

A unified view of the mechanisms governing superplastic behavior is evolving gradually. The existence of a number of rate controlling processes concurrent with a requisite fine structure is highly probable. From an analysis of strain rate hardening in Pb-Sn, Avery and Backofen **(32)**proposed that Nabarro-Herring diffusional creep and climb regulated dislocation motion are competing mechanisms. Later work by Packer and Sherby (34) cast doubt on the importance of Nabarro-Herring

creep as a rate controlling process. In eutectic Al-Cu, Holt and Backofen (31) proposed, from microstructural evidence and the grain size dependence of σ at constant $\dot{\varepsilon}$, that grain boundary shear coupled with strain rate enhanced recrystallization and boundary migration would account for the observed variation of m with $\dot{\varepsilon}$. Packer and Sherby (34) found indications of grain boundary migration or recrystallization in constant speed tests of Al-Zn eutectoid alloy. Grain size and shape were essentially unchanged with deformation.

In the present study, the anomalous ductility in extruded Co-45W-0.05Zr suggested a number of experiments to examine the role of grain size and phase transformation on strength and ductility.

Additional Experiments on Superplasticity

Variable strain rate tensile tests were conducted on the tapered end specimens illustrated in Figure 4(b). These were machined from extruded bars of both conventionally cast and unidirectionally solidified ingots of Co-45W-0.05Zr. Testing was performed at 1800°F on an Instron machine in a 16 inch long electric resistance furnace. The initial temperature variation along the 1.14 inch test section of less than 2°F was maintained

to elongations of at least 100%. The time required to bring the furnace and specimen up to 1800°F from room temperature was about 3 hours. An additional period of 1/2 hour at temperature preceded actual testing.

Following the procedure of Backofen, et. al. (27), transient tensile tests were conducted by increasing the pulling speed by factors of 2 or 2 1/2 over nearly three orders in magnitude and observing resulting changes in load. The crosshead speeds ranged from 0.002 to 2 inches per minute. Stress as a function of instantaneous strain rate was calculated assuming uniform reductions in cross section. The strain rate sensitivity was obtained from $\sigma = K \dot{\varepsilon}^m$ as follows:

$$\log \sigma = \log K + m \log \dot{\varepsilon}$$

$$m = \left(\frac{\partial \log \sigma}{\partial \log \dot{\varepsilon}}\right)_{\varepsilon}$$

In actuality, the increments are finite, thus

$$m = \left(\frac{\Delta \log \sigma}{\Delta \log \dot{\varepsilon}}\right)_{\varepsilon} = \left(\frac{\log \sigma_2 - \log \sigma_1}{\log \dot{\varepsilon}_2 - \log \dot{\varepsilon}_1}\right)_{\varepsilon}$$

$$= \left(\frac{\log \frac{\sigma_2}{\sigma_1}}{\log \frac{\dot{\varepsilon}_2}{\dot{\varepsilon}_1}}\right)_{\varepsilon}$$

Because m is measured at a common strain to eliminate the possible influence of strain hardening or other metallurgical change, the ratios of loads, P, and pulling speeds, V, may be used instead.

$$m_{\dot{\varepsilon}_1} = \left(\log \frac{P_2}{P_1} \Big/ \log \frac{V_2}{V_1} \right)_{\varepsilon}$$

where ε_1 and P_1 are the strain rate and load at the slower pulling speed V_1.

Figure 31 illustrates schematically the type of data obtained in these tests. With an increase in pulling speed, the load exhibited a transient rise and then remained nearly flat although at high speeds, it sloped appreciably downward. The curves of load versus time were extrapolated to obtain a common strain for the pulling speeds used in calculating a particular m. A given m value was associated with the strain rate at the lower pulling speed. For example, in Figure 31, ε_1 is given by $V_1 \div$ gage length at location (time) 1. Usually about 60% of strain was required for a set of measurements over the entire pulling speed range of. 002 to 2 inches per minute.

The grain size and intermetallic size and spacing were controlled through variations in cast structure. Test specimens taken from different positions of the extruded bars varied in .

structural fineness. This was particularly true of the unidirectionally solidified extrusions where the as cast structure was fine near the chill and became more coarse with distance. The gradation in cast structure was reflected in the extrusions and provided test material with a range of grain and intermetallic sizes.

The metallographic mean free path, L_{α}, between face centered cubic α grains was taken as a measure of structural fineness. A filar eyepiece was used to determine intercept distances of these grains, disregarding the intervening intermetallic. The average of 10 separate random determinations on 10 α phase grains in a row gave closely reproducible results. Contained implicitly in this measure of grain size is the size of the intermetallic since fine grained regions were invariably accompanied by fine and closely spaced W_6Co_7, while areas of coarse grains contained correspondingly large and coarsely spaced particles,

Some material was heat treated in evacuated Vycor tubes prior to testing. Standard metallographic techniques were used in preparing and examining both as extruded and tested material. Some of the chemical etchants described in Table I were utilized to delineate particular structural features.

Results and Discussion

Effect of $\dot{\varepsilon}$ on σ and m in As Extruded Material

Much larger elongations were obtained in the controlled tensile tests than in creep. After about 400% elongation, the temperature distribution along the specimen became extremely non uniform. Nevertheless, some very large neck-free elongations were observed, Figure 32.

Plots of flow stress, σ, and strain rate sensitivity index, m, versus $\dot{\varepsilon}$ for four different values of $L_{\alpha\gamma}$ appear in Figures 33 and 34. The lower L_α values of 1.6 and 2.0 microns are for material taken from the nose and end portion of a unidirectionally solidified and extruded ingot. The L_α values of 2.6 and 2.9 microns are for specimens corresponding to the bottom and center portions of a conventionally cast ingot. As stated previously, the extruded structures of unidirectionally solidified ingots were the more uniform of the two. Microstructures of extruded material have been described in an earlier section.

The flow stress at constant $\dot{\varepsilon}$ is dependent on L_α; σ increases with L_α, Figure 33. The slope of these lines, m, measured independently, varies appreciably with $\dot{\varepsilon}$, Figure 34.

The general trend in this figure is for m to increase with $\dot{\varepsilon}$. A peak in m is not apparent at higher $\dot{\varepsilon}$ except for the coarsest structure. This probably is a consequence of the tests being conducted at pulling speeds below 2 inches per minute; at higher pulling speeds, a peak in m would be expected. With decreasing $\dot{\varepsilon}$, m undergoes a minimum. All of the curves exhibited this minimum and for some there appears to be a small peak in m at low $\dot{\varepsilon}$.

An interpretation of the m-$\dot{\varepsilon}$ curves in Figure 34 merits caution at this time. To examine further the nature, and even perhaps authenticity, of a peak in m at lower $\dot{\varepsilon}$, obviously merits additional study over a wider range of strain rates than currently employed. Furthermore, the difficulties that become apparent in attempting to rationalize fully the grain size dependence of these m-$\dot{\varepsilon}$ curves probably stems from the actual measure of L_γ. For highly non uniform structures, such as some of those tested, L_γ, an average quantity, is not likely to provide a good indication of the overall test section strain rate sensitivity.

It also must be appreciated that these tests were conducted on non equilibrium structures which were transforming during deformation. The degree of transformation could be

expected to vary with time so that a larger ε (specimen subjected to longer time at 1800°F) the metallurgical condition of the material (amount of transformation, grain size, etc.) probably differed from that found earlier in the test.

Microstructural examination of tested specimens showed that considerable transformation had occurred during heating and the one hour at 1800°F. The reaction of σ and W_6Co_7 to form Co_3W has been recently established at 1093°C (2000°F) ± 5°C (18). The temperature of an additional peritectoid reaction in which ε forms has not been definitely found. Evidence exists that it may occur below 1050°C (18). After testing, all of the finer intermetallic particles of the type shown in Figures 27(a), (c) had dissolved leaving the original pointed voids. Traces of the larger particles still remained, Figure 35. The darker precipitate areas are probably a mixture of ε and α, the light areas being Co_3W.

After an m versus $\dot{\varepsilon}$ determination, samples were pulled at 2 inches per minute to failure. The elongations at fracture increased with decreasing $L_{a'}$ Thus, for L_a = 1.6, 2.0, 2.6, 2.9 µthe respective elongations were 535%, 215%, 139%, and 58%. The two coarsest grained specimens showed surface cracking. Tests to failure were not conducted at different constant strain

rates or pulling speeds. Accordingly, it is not clear whether fracture behavior or the particular m for the testing conditions regulated the ductility. Especially for the more non uniform material m, an average quantity, might disregard the relative brittleness of very coarse grains thereby giving an inaccurate indication of overall necking or early failure resistance.

Influences of Deformation History and Transformation

In order to examine the influence of previous strain and strain rate history, an as extruded specimen (unidirectional ingot, $L_\alpha \sim 1.8\mu$) was subjected to a series of m versus ε determinations. The cross head speed was increased from .002 to .2 inches per minute in seven steps and the process repeated for a total of four runs. The strain after each run was about 20%. After the final determination, the speed was raised to 2 inches per minute with fracture occurring at 415% elongation. The total time at temperature was 2 hours as compared to 1 hour used for the previously described tests.

The results of these tests are presented in Figures 36 and 37(a). The flow stress increased with successive runs, changing very slightly for the third to fourth. Similarly, the curves of m versus $\dot{\varepsilon}$ were essentially identical for the last

two runs. The very small random scatter in these curves may be taken as an indication of the accuracy of the m determinations for this specimen.

These results suggest that some sort of structural equilibrium was being approached through deformation. Both the flow stress and m curves imply a coarsening with repeated deformation and (or) time at temperature. Thus, the rise of flow stress with successive runs is indicative of a coarser structure as shown in Figure 33. A similar inference is provided by the m-ε curves in Figure 38(a). It has been found that the strain rate at peak m or at fixed values of m will shift to higher strain rates as structure becomes finer (31, 32). At low $\dot{\varepsilon}$ the curves in Figure 37(a) are almost flat and a shift to lower $\dot{\varepsilon}$, indicative of coarsening, is not apparent. However, at higher E the curves become more steep and their displacement to lower $\dot{\varepsilon}$ with successive runs is clearly evident. After the third run, this shift was extremely slight.

Metallographic examination of this sample showed that heavy precipitation had occurred. Figure 38 compares the microstructure in the grip ends and deformed region. The light areas are Co_3W, the precipitate areas are probably α and E. After considerable extension, the Co_3W grains remained equiaxed,

Figure 38(b), while the darker precipitate was strung out longitudinally. In general, the grains were delineated with considerable difficulty. The W_6Co_7 had not dissolved completely as shown in Figure 38(d). A large W_6Co_7 particle is surrounded by grains of Co_3W. Figure 38(d) shows one of the largest of many voids now elongated, that had originally defined the position of coarse as extruded W_6Co_7 particles (see Figure 27(d)). These voids did not propagate transversely, but merely extended on deformation in accordance with the overall necking resistance of the superplastic material.

To establish more clearly the role of phase transformation in this system, a specimen ($L_\alpha \sim 2\mu$, unidirectional ingot) was annealed at 1800° F for 100 hours* and subjected to the same series of transient tensile tests used for the previously described as extruded specimen, After three runs, it failed without necking after 52% elongation as m was decreasing rapidly, Figure 37(b). With the expection of the comparatively low elongation, probably associated with a sharp drop in m, the behavior of this sample was superplastic. Its response to speed changes in m-$\dot{\varepsilon}$

- - - - - - - - - - -

*The 100 hour time was chosen based on Neumier and Holman's work (18) which showed that for alloys containing 65-85 atomic % Co, equilibriation heat treatments at 900-1100° C in excess ,of 96 hours did not produce any additional structural changes.

determinations (see Figure 31)and absence of necking was identical to that observed for all other specimens.

The flow stress, Figure 36,did not exhibit a rise with successive runs as was the case for as extruded material. However, the curve of m vs $\dot{\varepsilon}$ did achieve a constant position after the first run at all but the highest strain rates, Figure 37(b). Thus, after the first run the curves for the second and third runs coincide almost exactly until a peak is reached. The attainment of a steady state through deformation is thus again suggested, this time in annealed material in which the contribution of transformation was either nil or at least greatly reduced. Therefore, the role of phase transformation does not appear to be a necessary condition for superplasticity, although diffusion during transformation represents a metastability which should contribute to lowering both the strength and viscosity.

In Figure 36, the substantially higher stresses in annealed material indicate a coarser structure than one characterized by $L_\alpha \sim 2\,\mu$ in the as extruded condition. This is the result of grain growth during prolonged exposure to 1800°F. The high m values of the annealed condition are probably the result of shifting the m-$\dot{\varepsilon}$ curves to the left. As discussed previously, such a shift is a further sign of coarsening. In Figure 37(a), no indication of

a peak in m exists at the highest strain rates.

After annealing, the interphase boundaries in undeformed regions were clearly defined, Figure 39(a)(c), and only two phases were present metallographically, ε (or α) and Co_3W. Following deformation, the Co_3W grains were not elongated, Figure 39(b)(d). The interphase boundaries, at least in Figure 39(d), became more rounded and distorted.

General Comments

This investigation on superplasticity, though limited, nevertheless establishes the existence of superplasticity in the Co-W system at the eutectic composition, Unlike more simple systems in which solid state transformations do not complicate the analysis, the Co-W system at 45 wt. % W undergoes a number of reactions. Thus, at about 2000° F, Co_3W forms by a peritectoid reaction from α and W_6Co_7 and at a lower temperature, as yet not definitely established Co_3W and α react to form ε . In spite of the uncertainties associated with the Co-W phase diagram at lower W contents and its reaction kinetics, some deductions are suggested by the results.

A number of conditions now generally regarded as desirable for obtaining superplasticity were present in this investigation. The test temperature of 1800° F was near a phase

boundary. Furthermore, this temperature was in excess of one half the absolute melting point, a desirable if not necessary condition. On extrusion, the intermetallic W_6Co_7 was aligned longitudinally, a less embrittling arrangement than found in cast material, and a very fine grain size was developed. And finally, the presence of compositional metastability, at least in unannealed material, could be expected to contribute to, if not solely determine, the superplasticity.

The data suggest that the necessity of phase transformation in superplasticity of Co-45W is secondary to that of a fine grain size. This latter condition appears to bean essential requirement for superplasticity. In as extruded material, larger elongations and lower flow stresses were obtained with finer grained samples, but the influence of grain size on m could not be clearly determined. Regardless of the details of the mechanisms involved in this alloy, continued recrystallization or grain boundary migration was probably occurring during deformation.

SUMMARY

Stress rupture tests of four Co-W base alloys cast in conventional investment molds and also unidirectionally solidified indicated a complex influence of cast structure on properties. The orientation of grain boundaries competed with the geometry, orientation and distribution of second phases in determining ductility and rupture life.

In general, ductility in the stress rupture test was higher for the unidirectionally solidified material, An exception to this behavior occurred with the Co-45W, 0.75Ti, 0.75 Zr, 0.25C, 0.1B alloy for which unidirectional solidification resulted in a very brittle arrangement of large carbide lamellae aligned nearly transversely to the direction of loading. For the Co-45W-0.05Zr and Co-45W, 0.75Ti, 0.75Zr, 0.25C, 0.1B alloys, unidirectional solidification led to improved rupture lives at lower stresses, while Co-35W-0.05Zr was markedly superior in the unidirectional condition over the entire stress range examined. Unidirectional solidification of Co-35W, 3Cr, 2Ti, 2Zr, 1C, 0.1B altered the microstructure considerably and produced segregation of MC carbides at the surface. The rupture life for this structure was inferior to that of the

conventionally cast alloy.

Extrusion of the above alloys in both cast conditions showed that Co-45W, 0.75Ti, 0.75Zr, 0.25C, 0.1B is not readily workable because of its coarse plate-like carbide structure. Of the other alloys extruded, only Co-35W-0.05Zr and Co-45W-0.05Zr yielded sound test material; the modified Co-35W alloy should be extruded at temperatures lower than those used to prevent embrittling overheating during working.

Stress rupture tests of the two unmodified alloys gave rupture lives nearly 100 fold lower than for cast material but large ductility increases.

The particularly large neck-free elongations observed for extruded Co-45W-0.05Zr led to an additional examination of superplasticity in this alloy. The results indicate the necessity of a fine structure for superplasticity with the role of phase transformation being secondary. Continued recrystallieation or grain boundary migration during tensile deformation is suggested by microstructural evidence.

LIST OF REFERENCES

1. R. L. Ashbrook and J. F. Wallace, "Modification of Eutectic Alloys for High Temperature Service", Trans. AIME, Vol. 236, 1966. p. 670.

2. R. J. Kissling and J. F. Wallace, "Grain Refinement of Aluminum Castings, Pt. 2", Foundry, Vol. 91, No. 7, July 1963, p.45.

3. V. B. Kurfman, "Nucleation Catalysis by Carbon Additions to Magnesium Alloys", Trans. AIME, Vol. 221, 1961, p. 540.

4. G. C. Gould, G. W. Form and J. F. Wallace, "Grain Refinement of Copper", Trans. AFS, Vol. 68, 1960, p. 258.

5. G. K. Turnbull, D. M. Patton and J. F. Wallace, "Grain Refinement of Steel Castings and Weld Deposits", Trans. AFS, Vol. 69, 1961, p. 792.

6. D. O. Stanley, "Effect of Solidified Structures on Mechanical Properties of Cast High Temperature Alloys", Ph. D. Thesis, Case Institute of Technology, June 1967.

7. R. W. Hertzberg, "Potential of Unidirectionally Solidified Eutectic Alloys as Reinforced Composites", Fiber Composite Materials, ASM, 1965, p. 77.

8. R. W. Hertzberg, F. D. Lemkey and J. A. Ford, "Mechanical Behavior of Lammelar ($Al-CuAl_2$) and Whisker Type ($Al-Al_3Ni$) Unidirectionally Solidified Eutectic Alloys", Trans. AIME, Vol. 233, Feb. 1965, p. 342.

9. R. H. Harrington, "A Survey of Alloy-Eutectic Sources for Aligned Structures", Watervliet Arsenal Rpt. No. WVT-6523, July 1964.

10. F. C. Lemkey, B. J. Bayles and M. J, Salkind, "Research Investigation of Phase-Reinforced High Temperature Alloys Produced Directly from the Melt", (United Aircraft Research Labs); U. S. Army Materials Research Agency, Technical Rept. No. AMRA-CR-64-0413, July 1965.

11. P. F. Weiser and J. F. Wallace, "Control of Cast Grain Size of Steel Castings - Effect of Structure and Nonmetallics on Properties", (Case Institute of Technology); U. S. Army Materials Research Agency, Technical Rept. No. AMRA-CR-64-0413, May 1967.

12. A. H. Cottrell, "Intercrystalline Creep Fractures" Structural Processes in Creep, London: Iron and Steel Institute, 1961, p. 1.

13. F. L. VerSnyder and R. W. Guard, "Directional Grain Structures for High Temperature Strength", Trans. ASM, Vol. 52, 1960, p.485.

14. B. J. Piearcey and F. L. VerSnyder, "A Breakthrough in Making Turbine Components. . .Directional Solidification and Single Crystals", Metal Progress, Nov. 1966, p. 66.

15. F. L. VerSnyder and B. J. Piearcey, "Single Crystal Alloy Extends Turbine Blade Service Life Four Times", SAE Journal, Aug. 1966, p. 36.

16. S. F. Ramseyer and J, F. Wallace, "Modified Eutectic Alloys for High Temperature Service", (Case Institute of Technology) Second Year Interim Rept. on NASA Grant SC-NsG 639/36-033-033.

17. M. Hansen and K. Anderko, Constitution of Binary Alloys, McGraw-Hill, New York, 1958.

18. L. A. Neumeier and J. L. Holman, "The Tungsten-Cobalt System for Compositions to 85 Atomic Percent Cobalt", Bureau of Mines Publication R1 6956, June 1967.

19. S. F. Ramseyer, "Control of Cast Structures of Alloys for High Temperature Service", Ph. D. Thesis, Case Institute of Technology, Nov. 1966.

20. R. Rautala and J. T. Norton, "Tungsten-Cobalt-Carbon System", Trans. AIME, Vol. 194, 1952, p. 1045.

21. L. D. Hunt and K. A. Jackson, "Binary Eutectic Solidification", Trans. AIME, Vol. 236, June 1966, p. 843.

22. I. S. Servi and N. J. Grant, "Creep and Stress Rupture Behavior of Aluminum as a Function of Purity", Trans. AIME, Vol. 191, 1951, p. 909.

23. F. C. Monkman and N. F. Grant, "An Empirical Relationship Between Rupture Life and Minimum Creel Rate in Creep-Rupture Tests", Proc. ASTM, Vol. 56, 1956, p. 593.

24. F. Garofalo, Fundamentals of Creep and Creep-Rupture In Metals, Macmillan, New York, 1965, p. 216.

25. Garofalo, p. 217-219.

26. H. Ll. D. Pugh and D. A. Gunn, "The Cold Extrusion of Brittle Materials Against a Hydrostatic Pressure", (Natl. Eng. Lab., East Kilbride, Scotland) NEL Rpt. 31, May 1962.

27. W. A. Backofen, I. R. Turner and D. H Avery, "Superplasticity in an Al-Zn Alloy", Trans. ASM, Vol. 57, 1964, p. 980.

28. C. E. Pearson, "The Viscous Properties of Lead-Tin and Bismuth-Tin", J. Inst. Metals, Vol. 54, 1934, p. 111.

29. E. E. Underwood, "A Review of Superplasticity", J. Metals, Vol. 14, 1962, p. 914.

30. E. R. Petty, "The Deformation Behavior of Some Aluminum Alloys Containing Intermetallic Compounds", J. Inst. Metals, Vol. 91, 1962-63, p. 274.

31. D. L. Holt and W. A. Backofen, "Superplasticity in the Al-Cu Eutectic Alloy", Trans. ASM, Vol. 59, 1966, p. 755.

32. D. M. Avery and W. A. Backofen, "A Structural Basis for Superplasticity", Trans. ASM, Vol. 58, 1965, p. 551.

33. J. D. Lubahn and R. P, Felgar, Plasticity and Creep of Metals, Wiley, New York, 1961.

34. C. M. Packer and O. D. Sherby, "An Interpretation of the Superplasticity Phenomenon in Two-Phase Alloys", Trans. ASM, Vol. 60, 1967, p. 21.

TABLES

TABLE I

List of Chemical Etchants Used in Metallographic Sample Preparation

Etchant	Composition	Remarks
1	50 cc HCl, 25 cc HNO_3, 1 gm $CuCl_2 \cdot 2H_2O$, 150 cc H_2O	Dip
2	100 cc HCl, 50 cc HNO_3, 50 cc H_2O, 10 cc 30% H_2O_2	"
3 *	1 vol part conc NH_4OH + 3 vol parts 30% H_2O_2	"
4*	28 gm $(NH_4)_2S_2O_8$ in 100 cc distilled H_2O	Dip, 50° to 80° C
5	conc. aqueous soln. of KOH (stain removal only)	Dip

*From Reference (18)

TABLE II

Representative Chemical Analyses

Chemical Analysis(wt. %)

Alloy (Aim, wt. %)	Co	W	Cr	Ti	Zr	C	B
Co-35W, 3 Cr, 2Ti, 2Zr, 1C, 0 1B							
conventional cluster	57 6	-	-	1. 98	2. 13	1. 00	. 09
unidirectional cluster	-	-	3. 22	1. 92	1. 96	. 98	. 10
conventional ingot	-	-	-	2. 06	1. 95	1. 10	. 080
unidi rectional ingot	-	-	-	-	2. 07	1. 04	-
Co-5W, 0. 75 Ti, 0. 75Zr, 0. 25C, 0 1B							
conventional cluster	54. 23	-	-	0. 80	0. 76	0. 25	0. 10
unidirectional cluster	-	-	-	0. 88	0. 62	0. 28	0. 10
conventional ingot	-	-	-	0. 81	0. 81	0. 30	0. 086
unidirectional ingot	-	-	-	0. 78	0. 73	0. 31	0. 090
Co-35W-0. 05Zr							
conventional cluster	-	-	-	-	0. 032	-	-
conventional ingot	-	-	-	-	0. 005	-	-
unidirectional ingot	-	-	-	-	0. 011	-	-
Co-5W-0. 05Zr							
conventional cluster	-	-	-	-	0 034	-	-

TABLE III

Stress Rupture Test Data For As Cast Alloys

Alloy Composition (Nominal wt. %)	Temp. °F	Initial Stress psi	Time to Fracture, Hours	Elongation %	Minimum Creep Rate 10^{-3} in/in-hr
Co-35W-0.05Zr (conventional)	1800	12,500	49.8	8.8	.952
	"	15,000	45.9	10.4	1.37
	"	17,500	15.9	16.0	6.43
	"	20,000	7.5	12.0	10.3
	"	25,000	1.8	8.8	48.0
Co-35W-0.05Zr (unidirectional)	1800	15,000	69.5	12.0	N.D.*
	"	15,000	128.1	16.0	N.D.*
	"	15,000	63.2	11.2	1.21
	"	20,000	23.7	12.0	5.20
	"	25,000	6.3	17.6	31.2
Co-45W-0.05Zr (conventional)	1800	10, 000	12.2	8.0	3.75
	"	15, 000	3.7	5.6	14.3
	"	20, 000	1.7	7.2	48.0
Co-45W-0.05Zr (unidirectional)	1800	10, 000	12.5	17.6	4.56
	"	12, 500	4.8	10.4	12.9
	"	15, 000	2.5	14.4	16.5
	"	20, 000	.40	8.0	120
	"	20, 000	.35	11.2	111

*N. D. -Not Determined

TABLE III (continued)

Alloy Composition (Nominal wt. %)	Temp. °F	Initial Stress psi	Time to Fracture, Hours	Elongation %	Minimum Creep Rate 10^{-3} in/in-hr
Co-45W, 0.75Ti, 0.75Zr, 0.25C, 0.1B (conventional)	1800	12,500	55.1	21.6	1.2
	"	15,000	37.8	16.8	1.83
	"	17,500	30.1	19.2	2.86
	"	20,000	21.5	17.6	N.D.*
Co-45W, 0.75Ti, 0.75Zr, 0.25C, 0.1B (unidirectional)	1800	12,500	81.9	6.4	.315
	"	15,000	55.9	7.2	.908
	"	17,500	24.3	5.6	1.78
	"	20,000	3.1	4.0	5.80
	"	20,000	5.9	3.2	7.56
Co-35W, 3Cr, 2Ti, 2Zr, 1C, 0.1B (conventional)	1850	17,500	70.9	23.2	1.61
	"	17,500	88.7	34.4	N.D.*
	"	20,000	51.4	28.8	N.D.*
	"	25,000	17.0	24.0	13.3
Co-35W, 3Cr, 2Ti, 2Zr, 1C, 0.1B (unidirectional)	1850	15,000	126.6	41.6	.784
	"	17,500	71.6	32.8	N.D.*
	"	20,000	27.7	27.2	3.78
	"	25,000	9.1	30.4	14.6

*N.D. -Not Determined

TABLE IV

Extrusion Data

	Billet No. (see Fig. 23)	Alloy & Cast Condition		Temp. °F	Ram Pressure, ksi		Ram Speed, in/sec
					Maximum	Run	
(a)	1	Co-35W-0.05Zr	conventional	2125	168.6	150.8	1.5
	2	" "	unidirectional	2150	162.5	142.0	1.8
	3	Co-35W-Modified	conventional	2150	164.2	128.7	1.0
	4	" "	unidirectional	2150	137.6	115.4	1.2
	5	Co-45W-0.05Zr	unidirectional	2200	173.1	137.6	4.8
	6	" "	unidirectional	2200	159.8	133.2	1.8
	7	" "	conventional	2200	164.2	124.3	1.8
(b)	1	Co-45W-Modified	conventional	2200	-	124.3	6
	2	" "	conventional	2150	168.6	133.2	1.8
	3	" "	unidirectional	2100	Stalled in press; re-extruded through .885" diameter die		
	3	" "	unidirectional	2125	162.0	119.8	2.2

TABLE V

Stress Rupture Test Data for Extruded All

Alloy Composition (Nominal wt. %)	Cast Condition	Temp. °F	Initial Stress psi	Time to Fracture, Hours	% Elongation
Co-35W-0.05Zr	conventional	1800	15,000	1.0	82.6
	"	"	20,000	0.4	43.4
	unidirectional	"	10,000	0.65	174
Co-45W-0.05Zr	conventional	"	7,500	0.17	96
	unidirectional	"	7,500	0.075	212*
	"	"	15,000	0.01	178
Co-35W-3Cr-2Ti-2Zr-1C-0.1B	conventional	1850	25,000	<0.01	6

*Did not break but exceeded test machine extension limit.

FIGURES

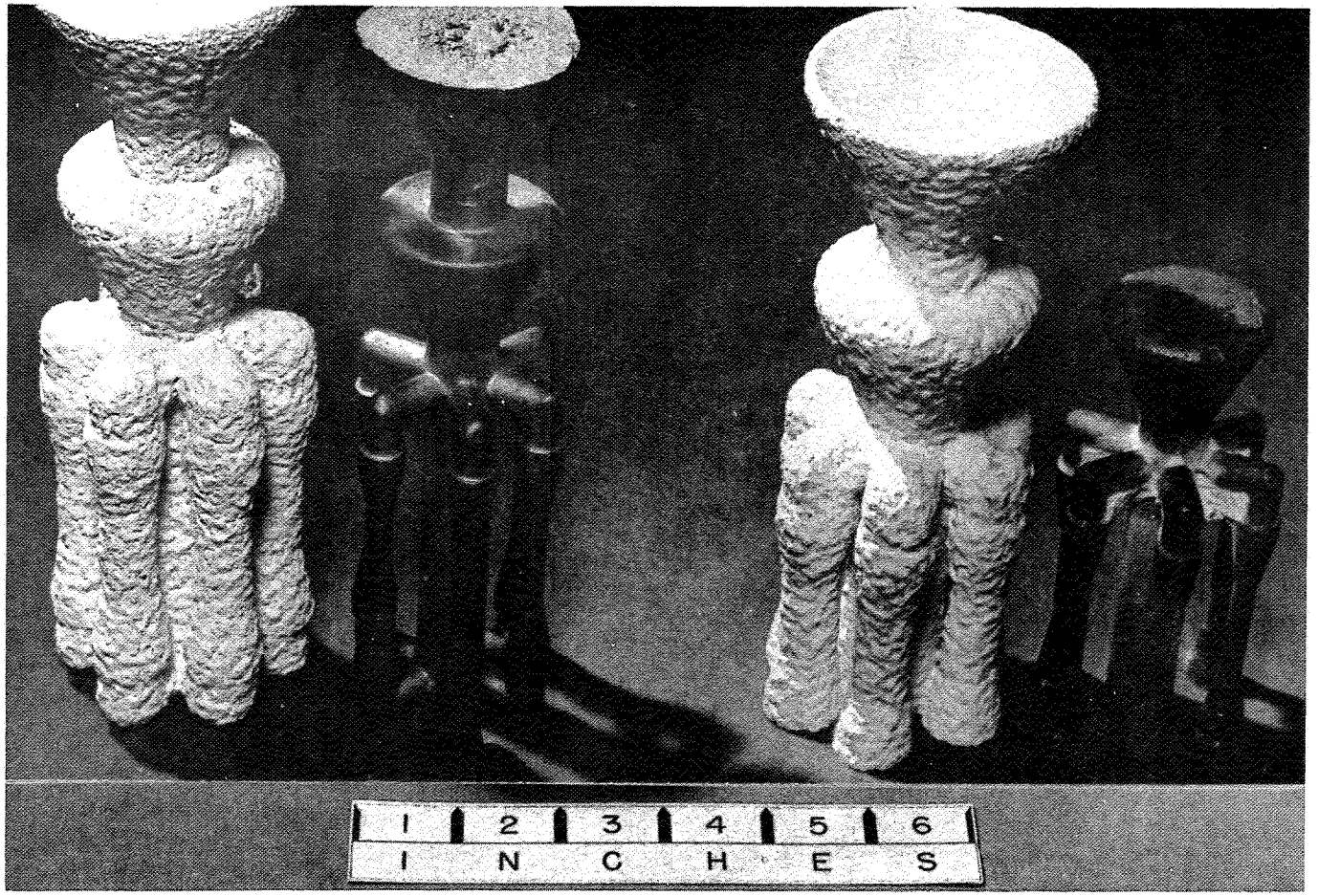

(a) (b)

Figure 1: Ceramic Molds and Clusters of As Cast Specimens; (a) Conventionally Cast, (b) Unidirectionally Solidified.

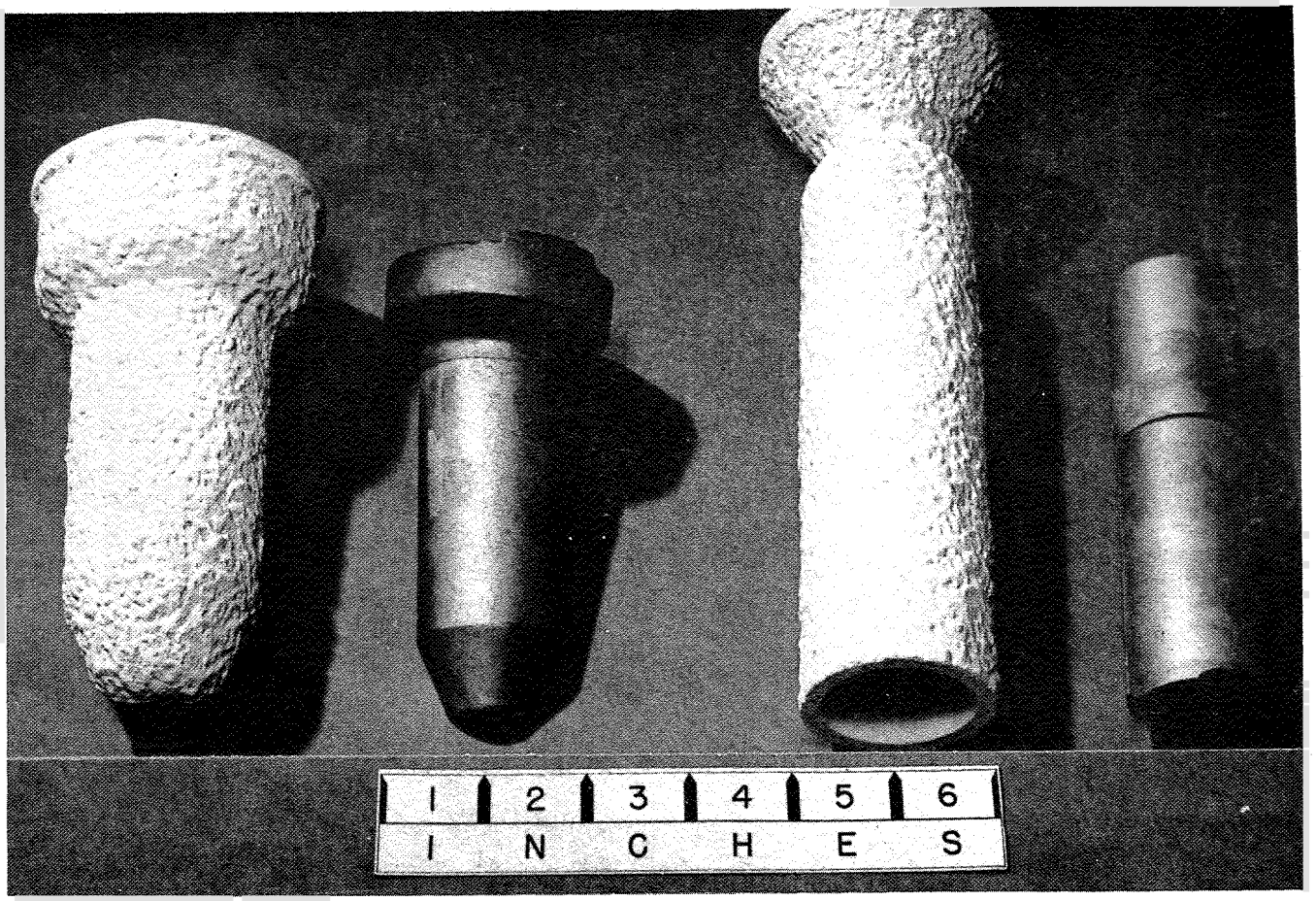

Figure 2: Two Types of Ingots Produced in Ceramic Molds, (a) Conventionally Cast (b) Unidirectionally Solidified.

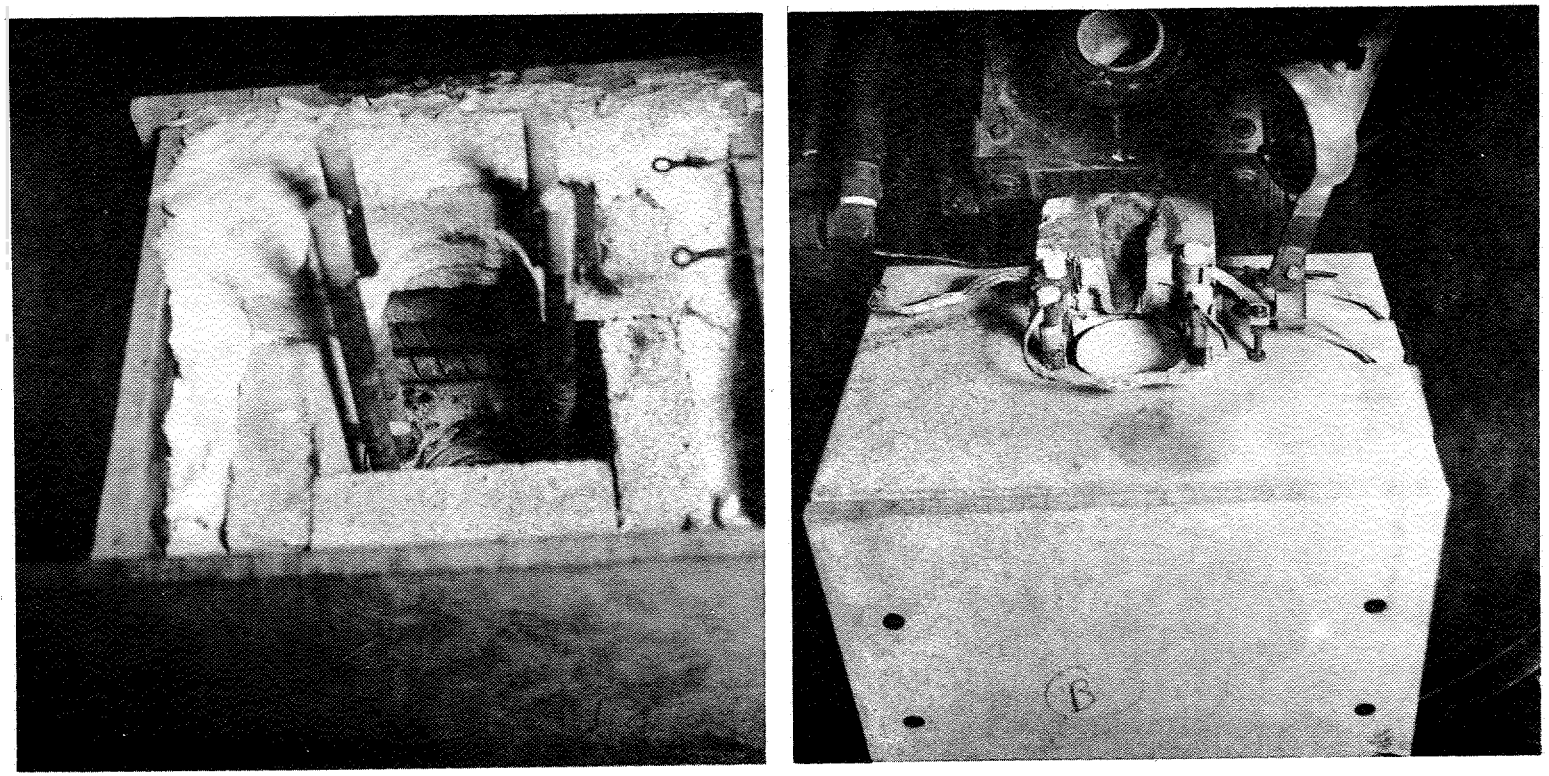

(a) (b)

Figure 3: Mold Furnace Used in Obtaining Unidirectional Solidification;
(a) Interior Detail Showing Insulation, Heating Elements, and Part of Copper Chill
(b) Assembly View With Mold in Place, Hold Down Weight Swung Aside and Induction Furnace in Background.

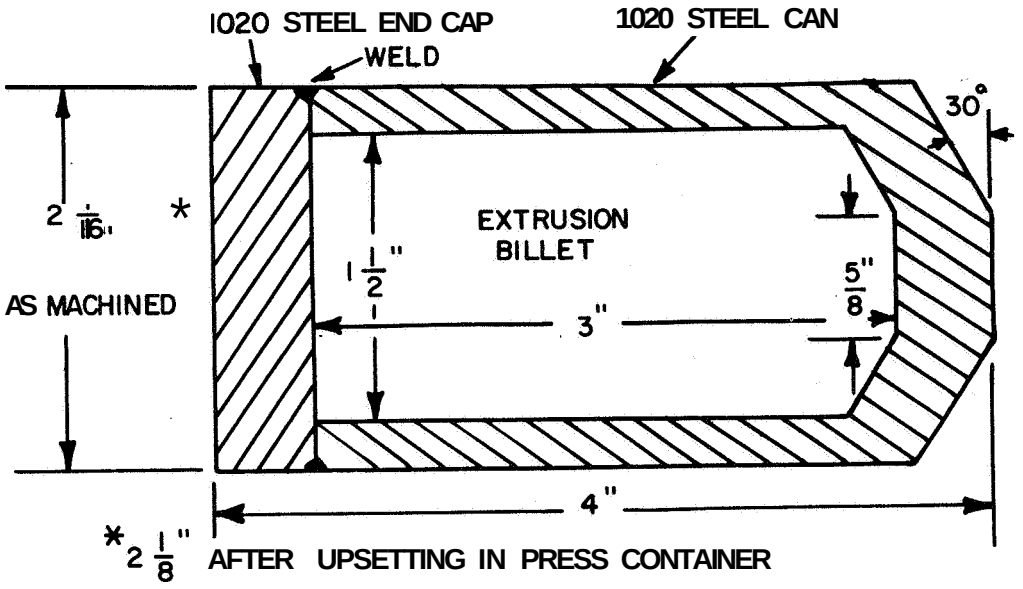

a) EXTRUSION BILLET AND CAN

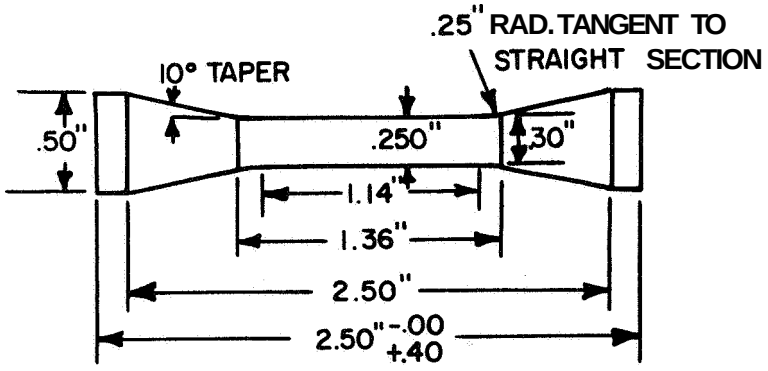

b) STRESS RUPTURE AND TENSILE SPECIMEN

FIGURE 4: DIMENSIONS OF EXTRUSION BILLET WITH CAN AND TEST SPECIMENS.

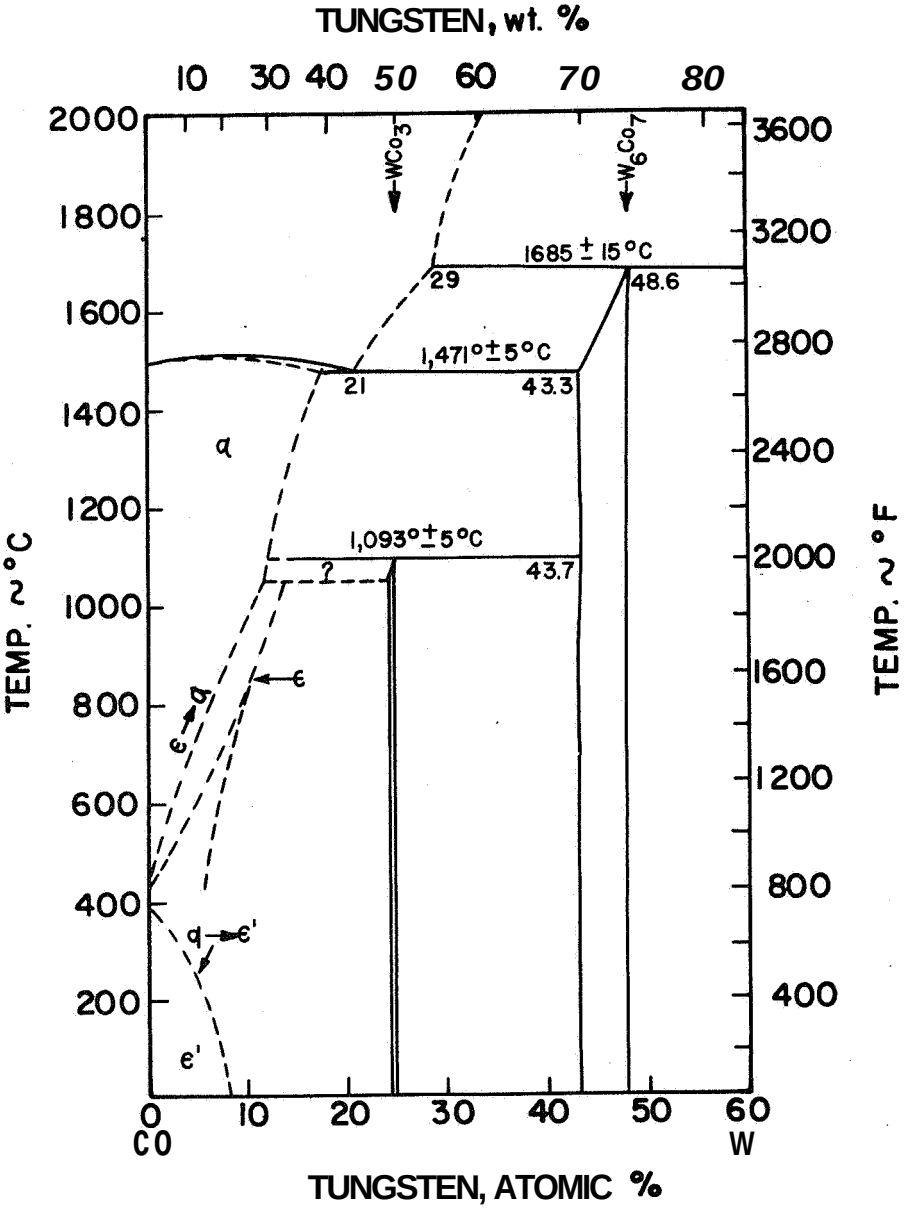

FIGURE 5 : THE Co – W SYSTEM (REF. 17, 18). DIAGRAM REDRAWN FROM REF. 18, OMITTING REGION ABOVE 60 ATOMIC % W.

(a) Conventional

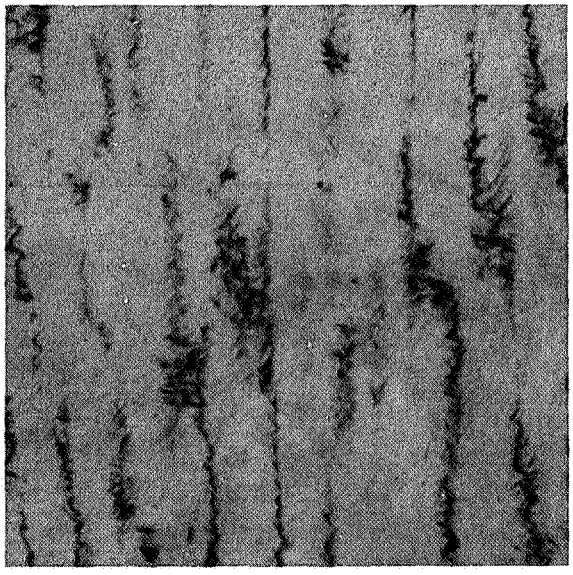

(b) Unidirectionally Solidified (Vertically)

Figure 6: Microstructure of Co-35W-0.05Zr From Test Sections of Stress Rupture Specimens (Etchant 1) 100X.

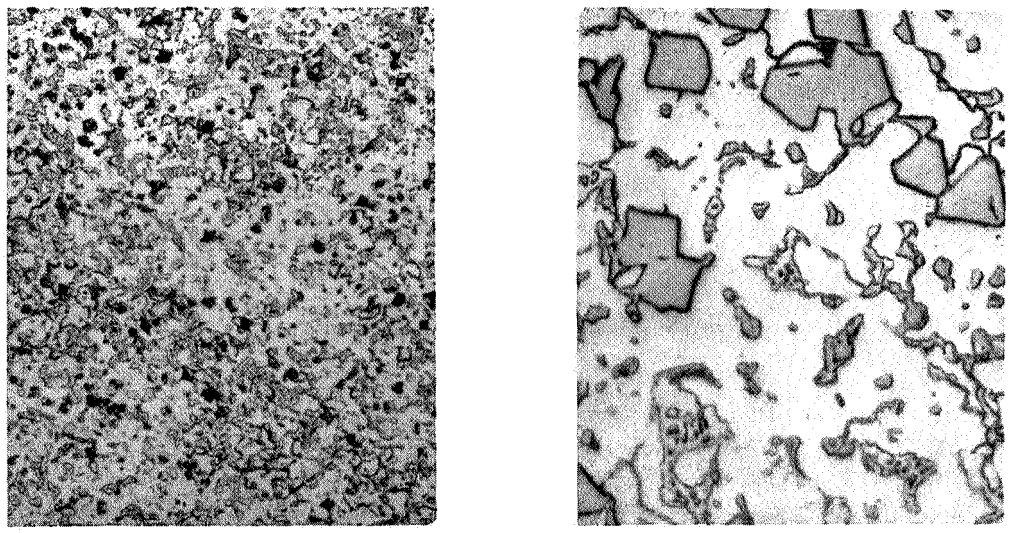

(a) 100X (b) 500X

Conventionally Cast

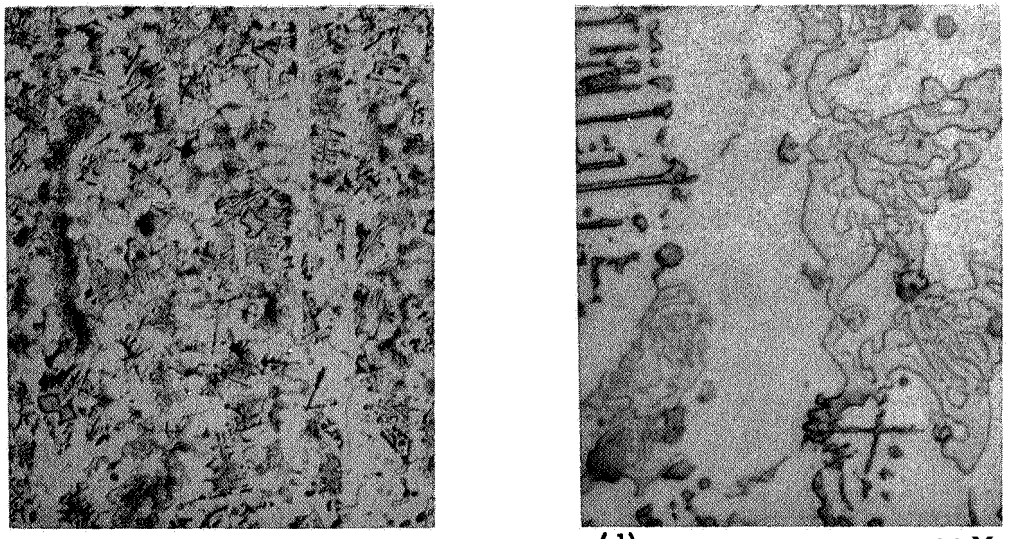

(c) 100X (d) 500X

Unidirectionally Solidified (Vertically)

Figure 7: Microstructure of Co-35W, 3Cr, 2Ti, 2Zr, 1C, 0.1B From Test Sections of Stress Rupture Specimens (Etchant 1).

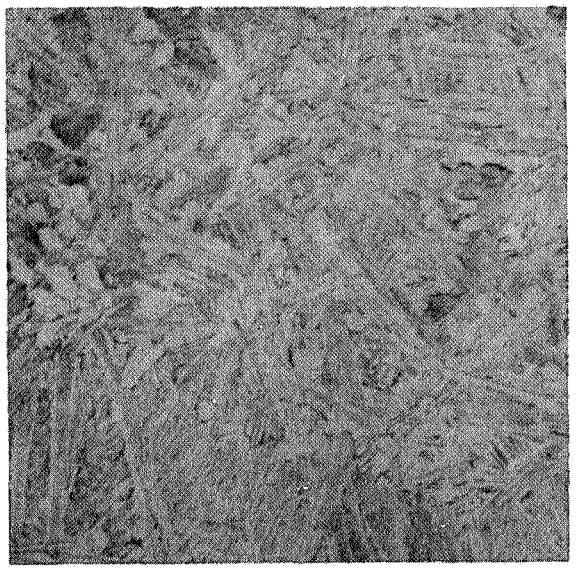

(a) Conventional

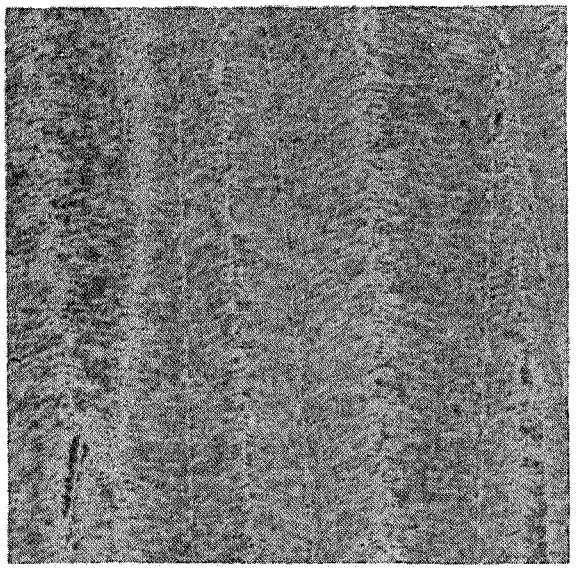

(b) Unidirectionally Solidified
(Vertically Upward)

Figure 8: Microstructure of Co-45W-0.05Zr From Test Sections of Stress Rupture Specimens (Etchant 1) 100X.

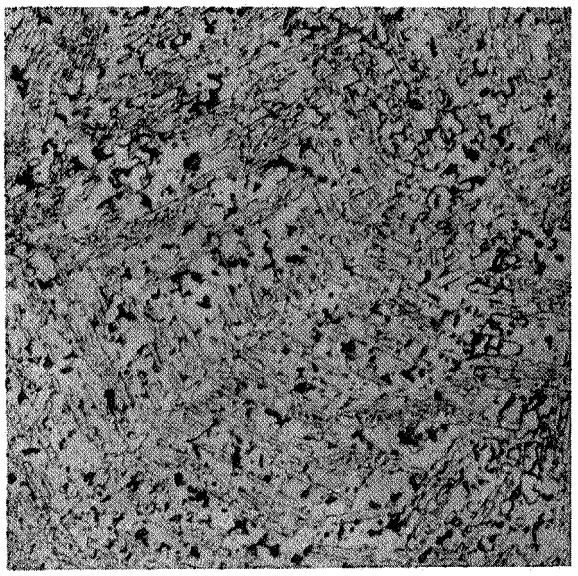

(a) Conventional

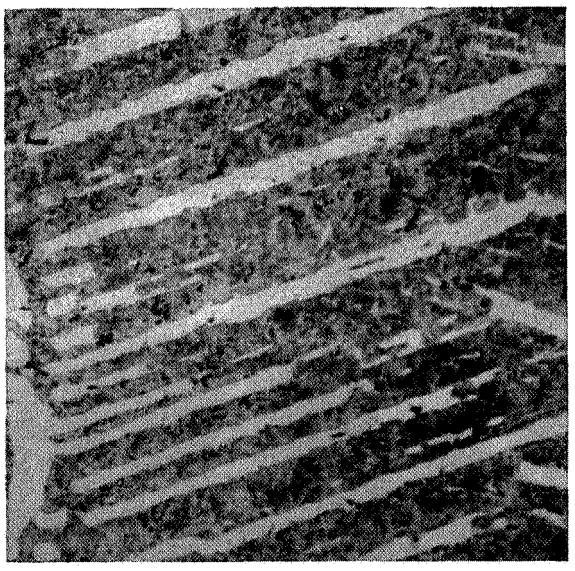

(b) Unidirectionally Solidified
(Vertically Upward)*

Figure 9: Microstructure of Co-45W, 0.75Ti, 0.75Zr, 0.25C, 0.1B From Test Sections of Stress Rupture Specimens (Etchant 1) 100X (*After Testing).

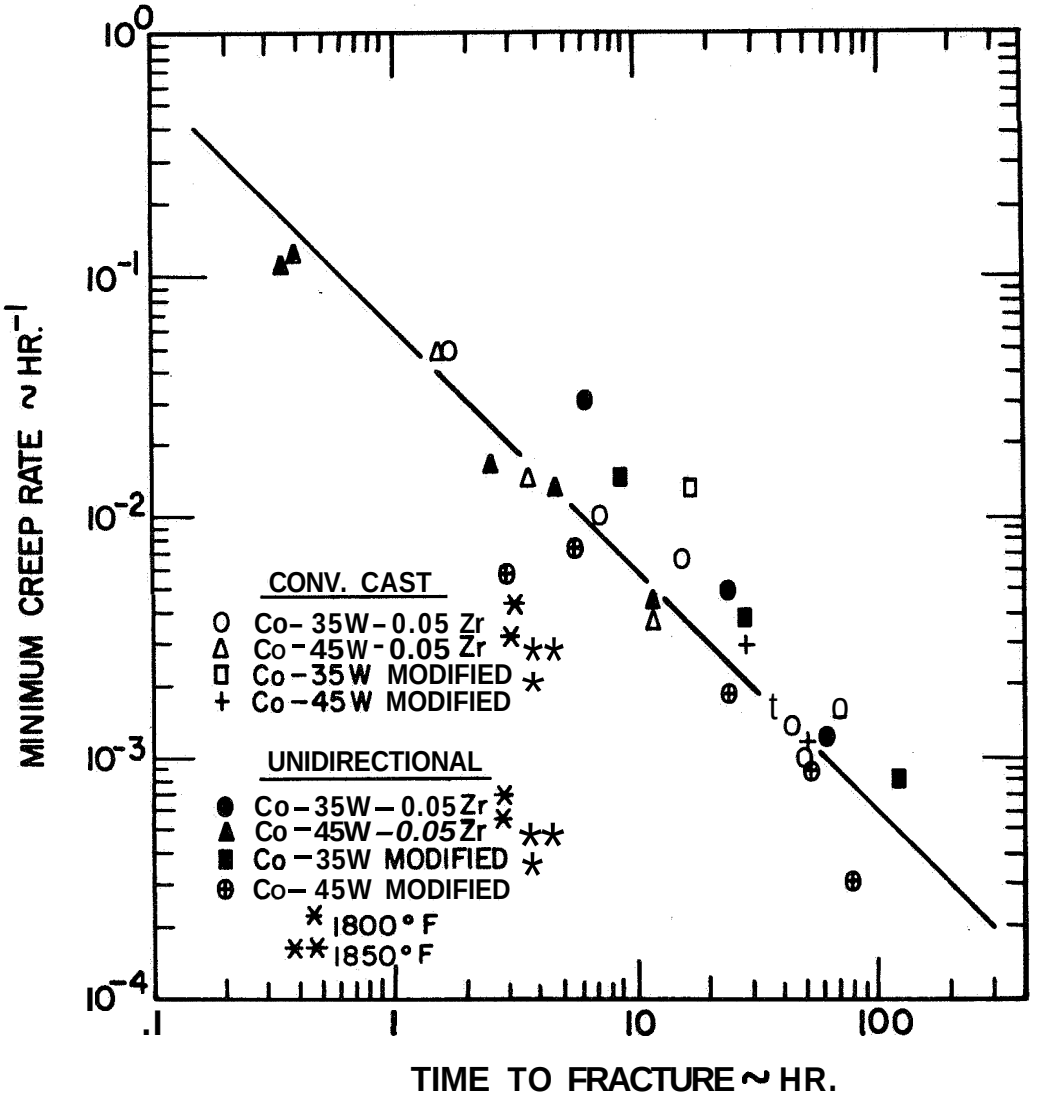

FIGURE 10 : RELATION BETWEEN STRESS RUPTURE LIFE AND MINIMUM CREEP RATE FOR ALL ALLOYS INVESTIGATED.

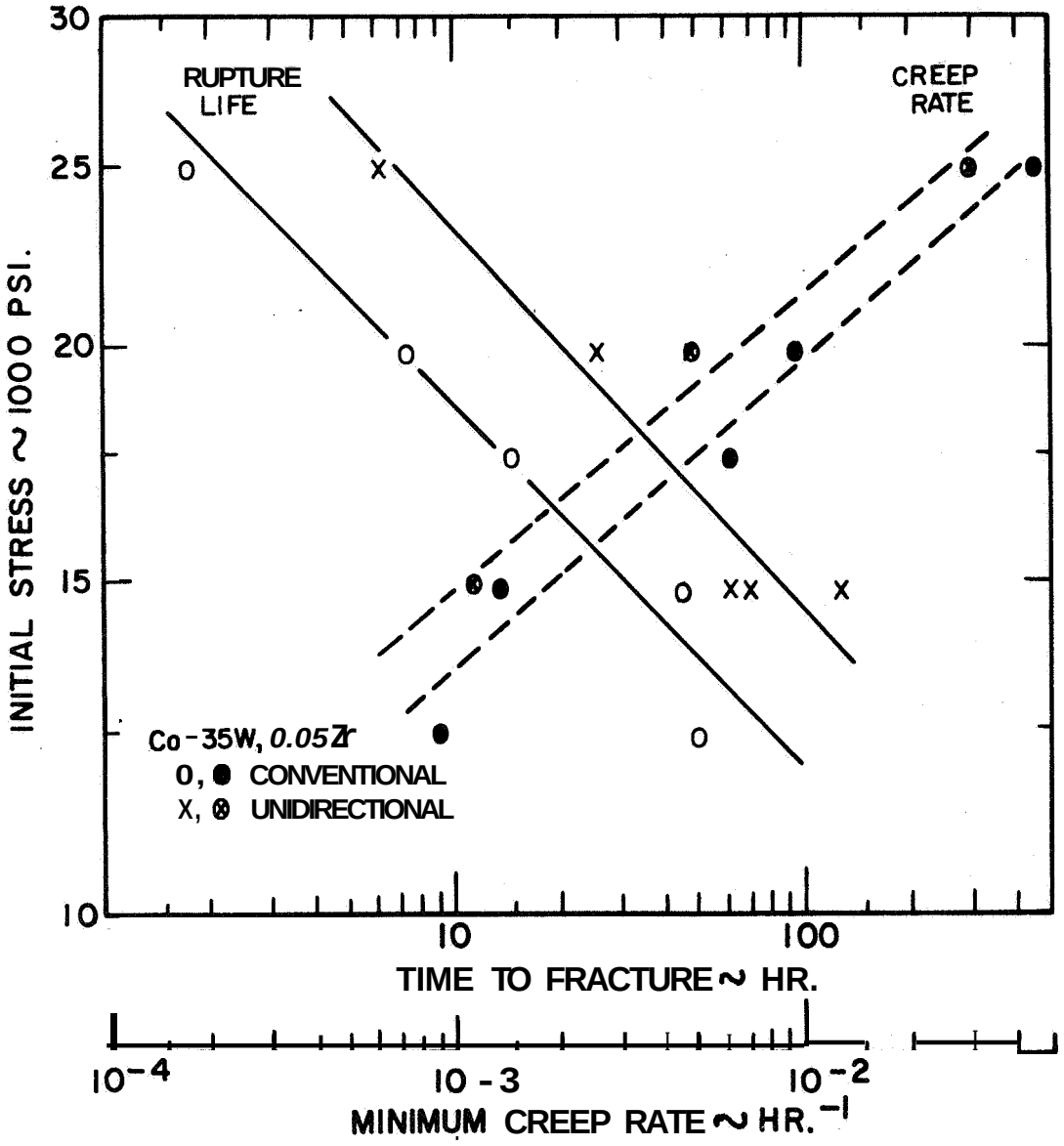

FIGURE 11: INFLUENCE OF CAST STRUCTURE ON RUPTURE LIFE AND MINIMUM CREEP RATE OF Co—35W, 0.05 Zr (TESTED IN AIR AT 1800° F).

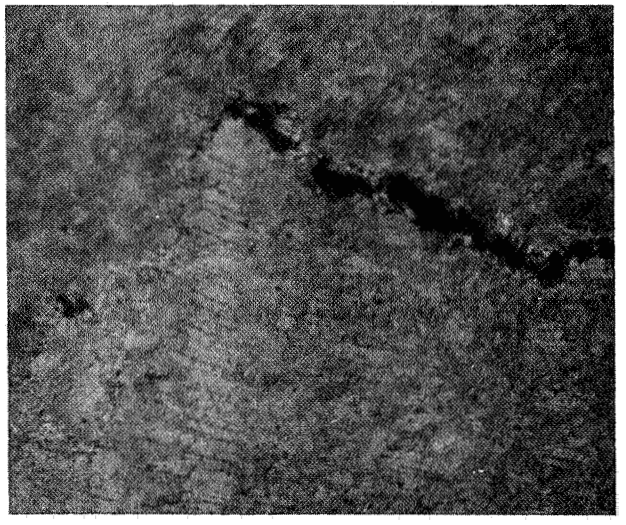

(a) Conventionally Cast

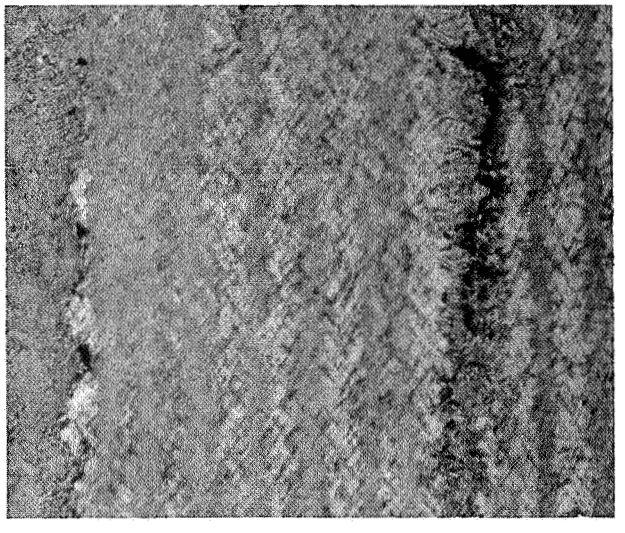

(b) Unidirectionally Solidified (Vertically)

Figure 12: Microstructure of Co-35W-0.05Zr After Stress Rupture Testing (Etchant 1) 100X.

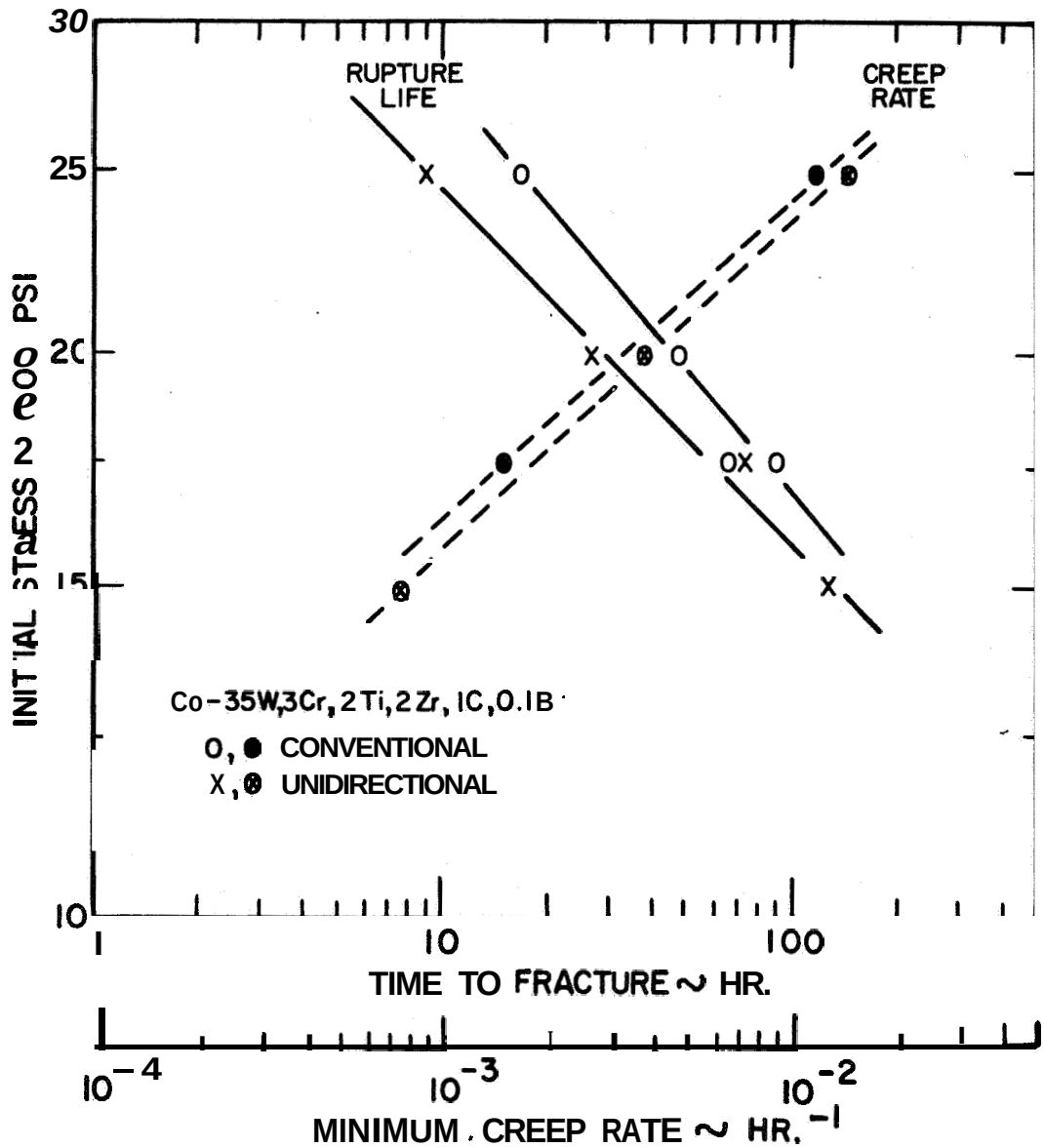

FIGURE 13: INFLUENCE OF CAST STRUCTURE ON RUPTURE LIFE AND MINIMUM CREEP RATE OF Co – 35 W, 3 Cr, 2 Ti, 2 Zr, 1C, 0.1B (TESTED IN AIR AT 1850° F).

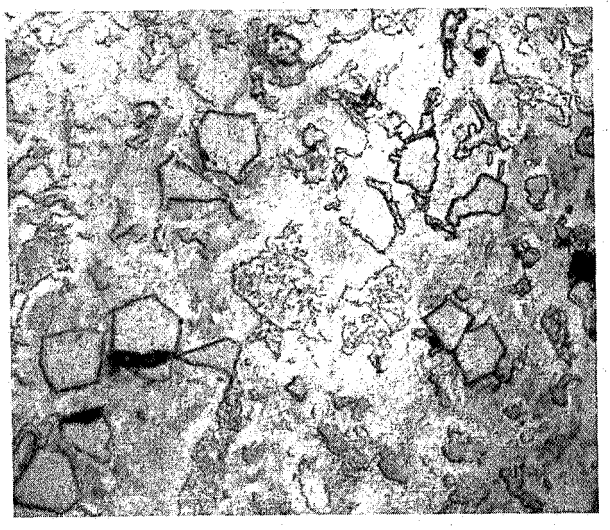

(a) 500X

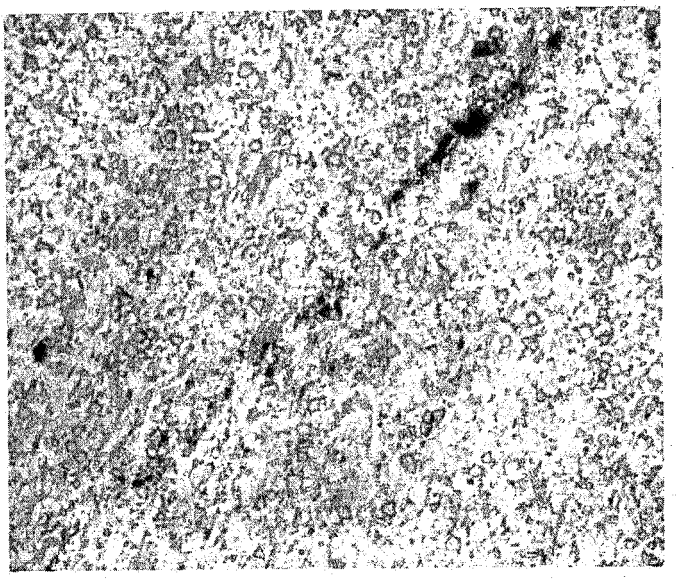

(b) 100X

Figure 14: Void Initiation in Co-35W, 3Cr, 2Ti, 2Zr, 1C, 0.1B Alloy (Etchant 1)

(a) Voids at Carbides in Conventionally Cast Alloy
(b) Grain Boundary Sliding in Conventionally Cast Alloy

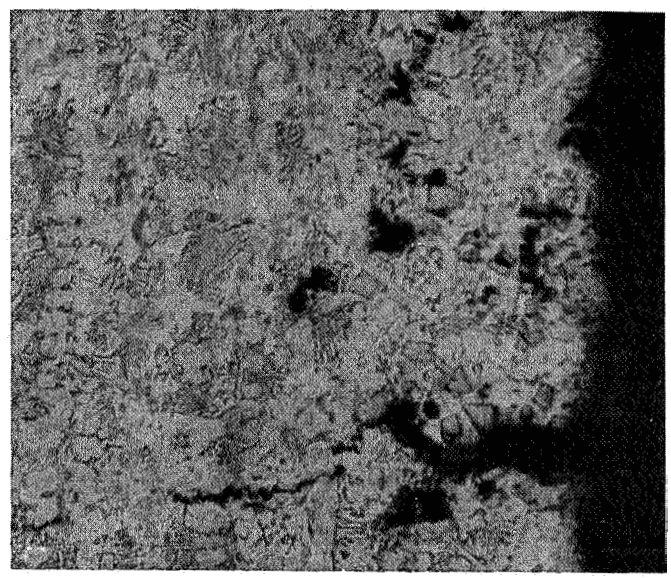

(c) 100X

Figure 14 (continued)

(c) Void Initiation at Carbide Clusters in Unidirectionally Solidified Alloy,

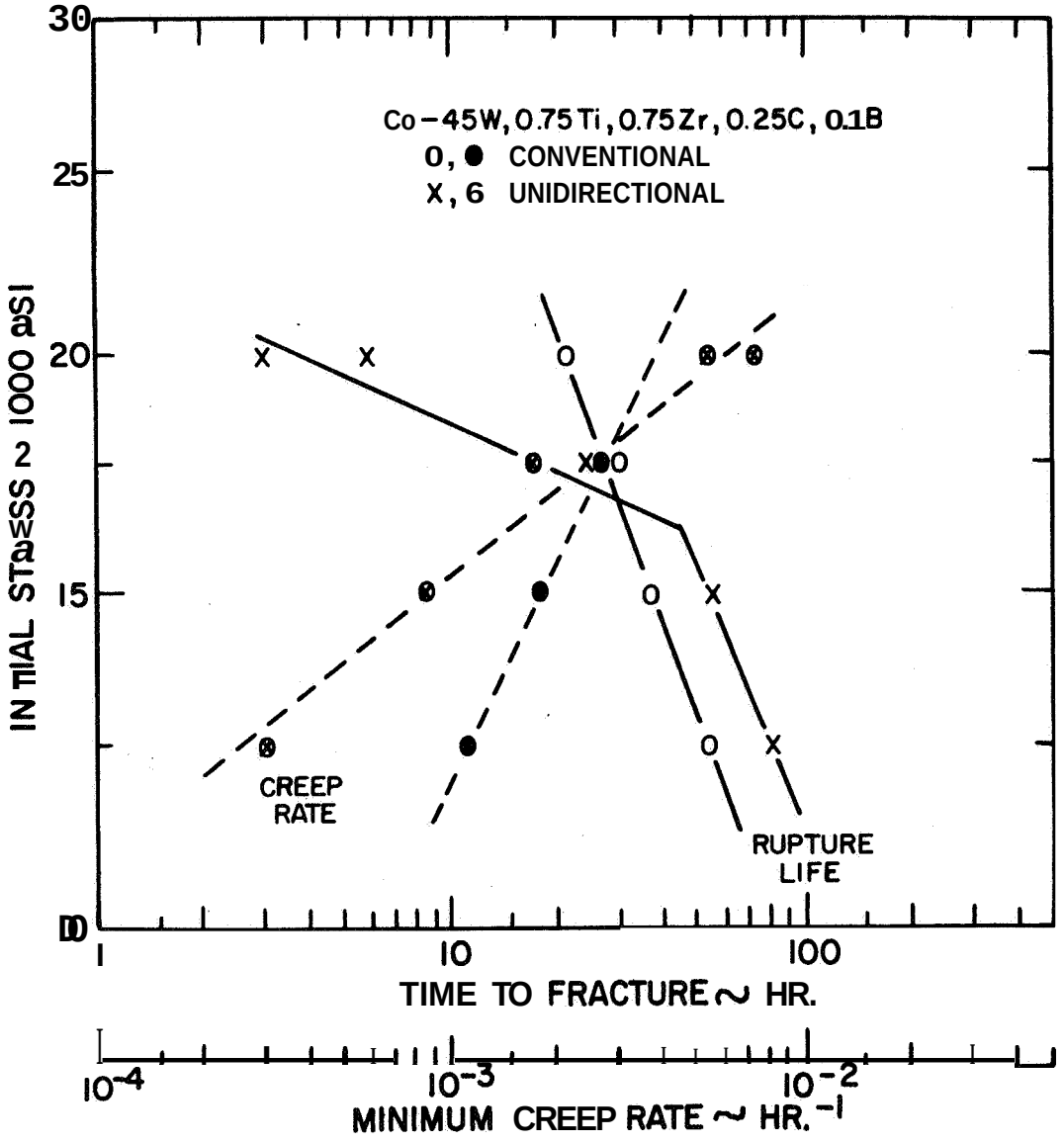

FIGURE 15: INFLUENCE OF CAST STRUCTURE ON RUPTURE LIFE AND MINIMUM CREEP RATE. OF Co-45W, 0.75Ti, 0.75Zr, 0.25C, 0.1B (TESTED IN AIR AT 1800°F).

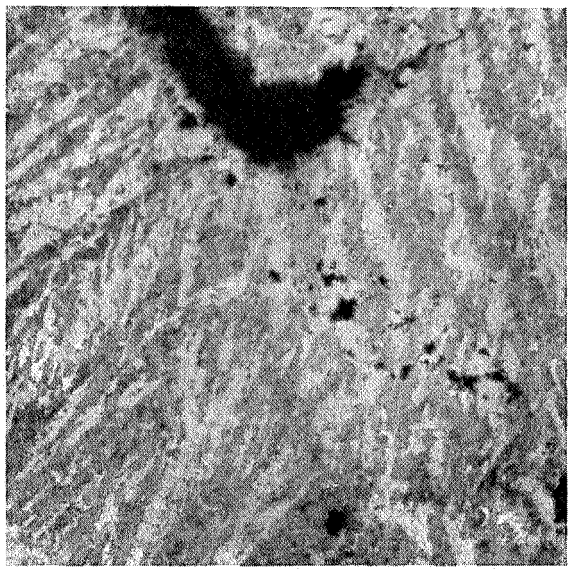

(a) 100 X

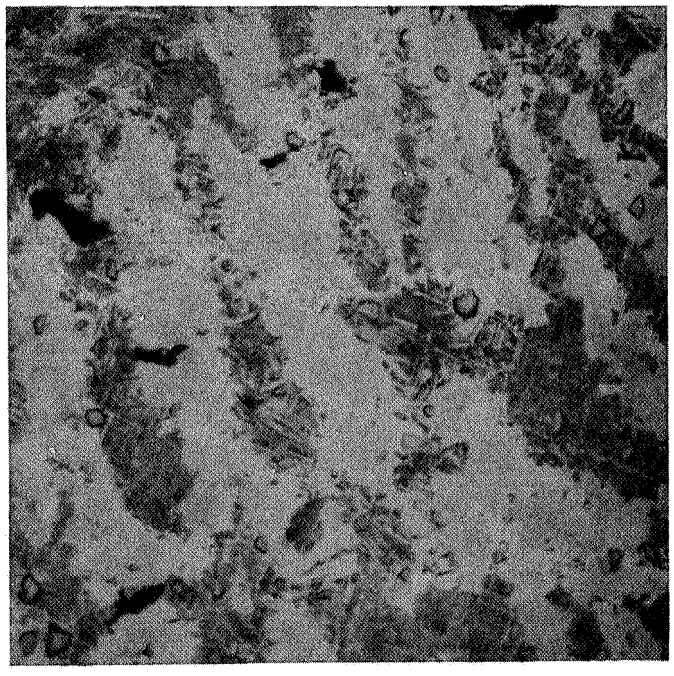

(b) 500 X

Figure 16: Types of Voids Observed in Tested Conventionally Cast Co-45W, 0.75Ti, 0.75Zr, 0.25C, 0.1B (Etchant 1).

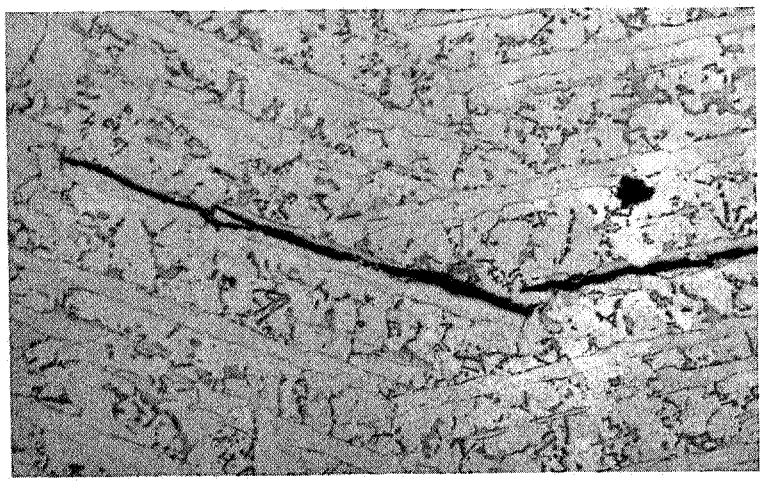

(a) 20,000 psi Testing Stress

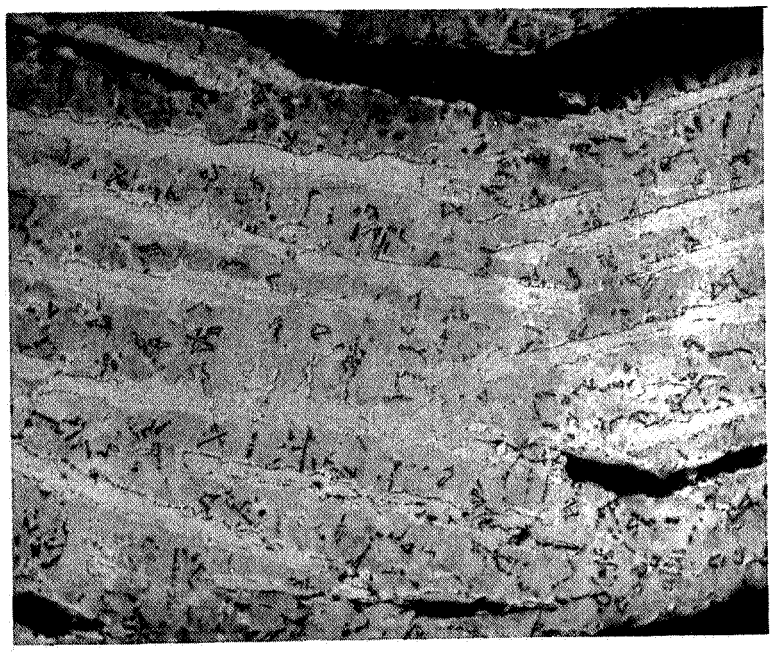

(b) 12,500 psi Testing Stress (Near Fracture Surface)

Figure 17: Cracks Initiated by Carbides in Unidirectionally Solidified Co-45W, 0.75Ti, 0.75Zr, 0.25C, 0.1B Alloy (Etchant 1) 100 X.

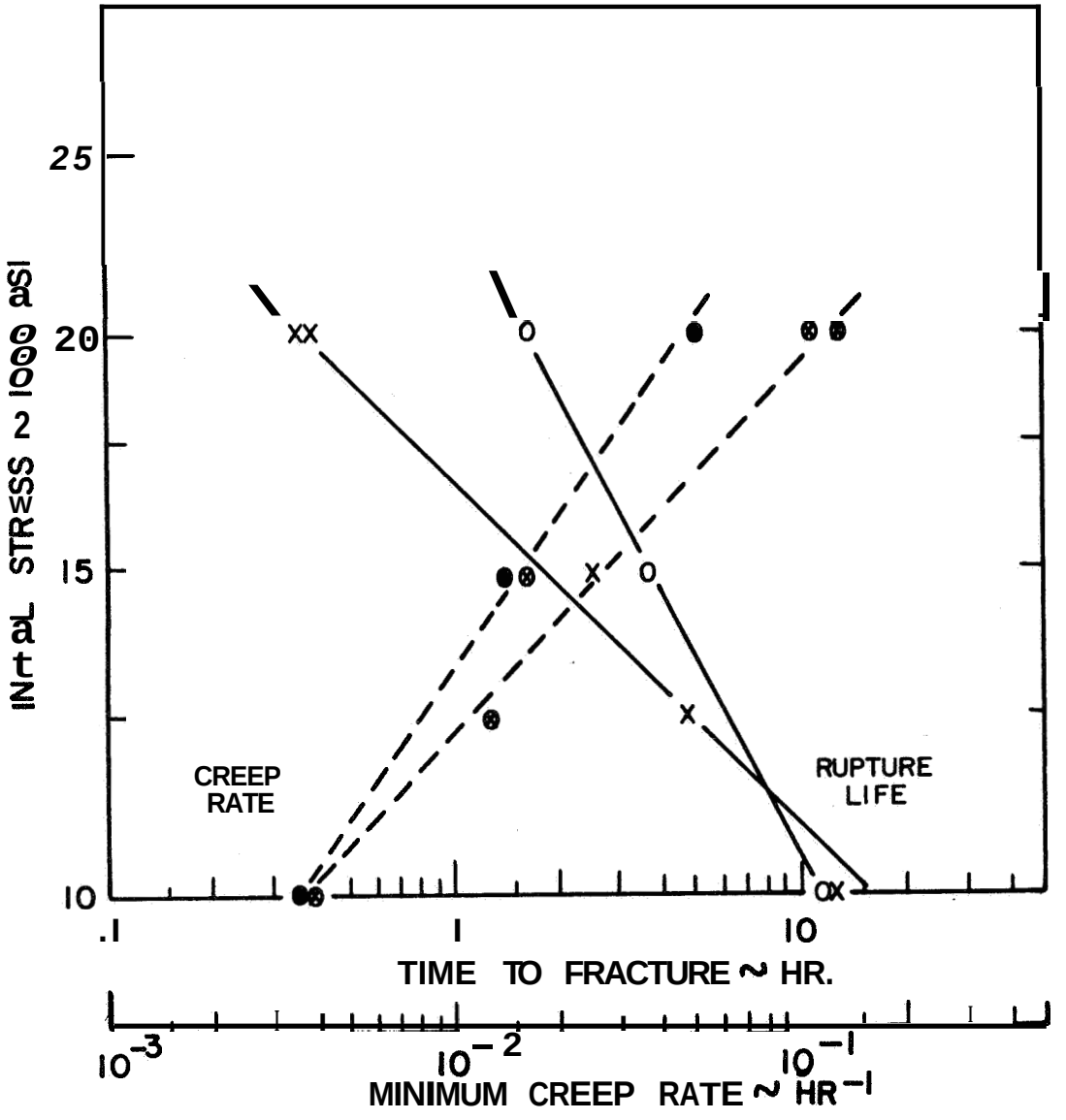

FIGURE 18 : INFLUENCE OF CAST STRUCTURE ON RUPTURE LIFE AND MINIMUM CREEP RATE OF Co–45 W, 0.05 Zr (TESTED IN AIR AT 1800 °F).

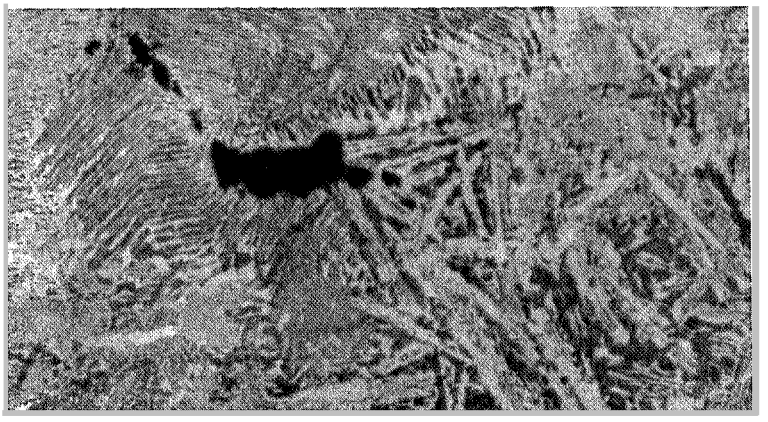

(a) Conventionally Cast

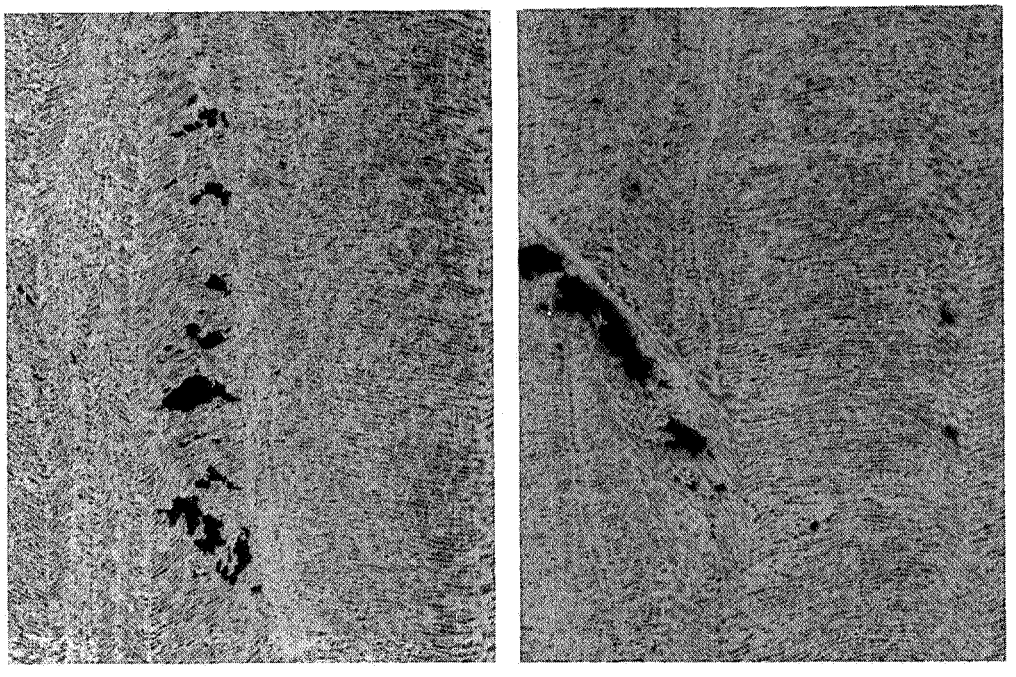

(b, c) Unidirectionally Solidified

Figure 19: Types of Voids Observed in Tested Co-45W-0.05Zr (Etchant 1) 100 X.

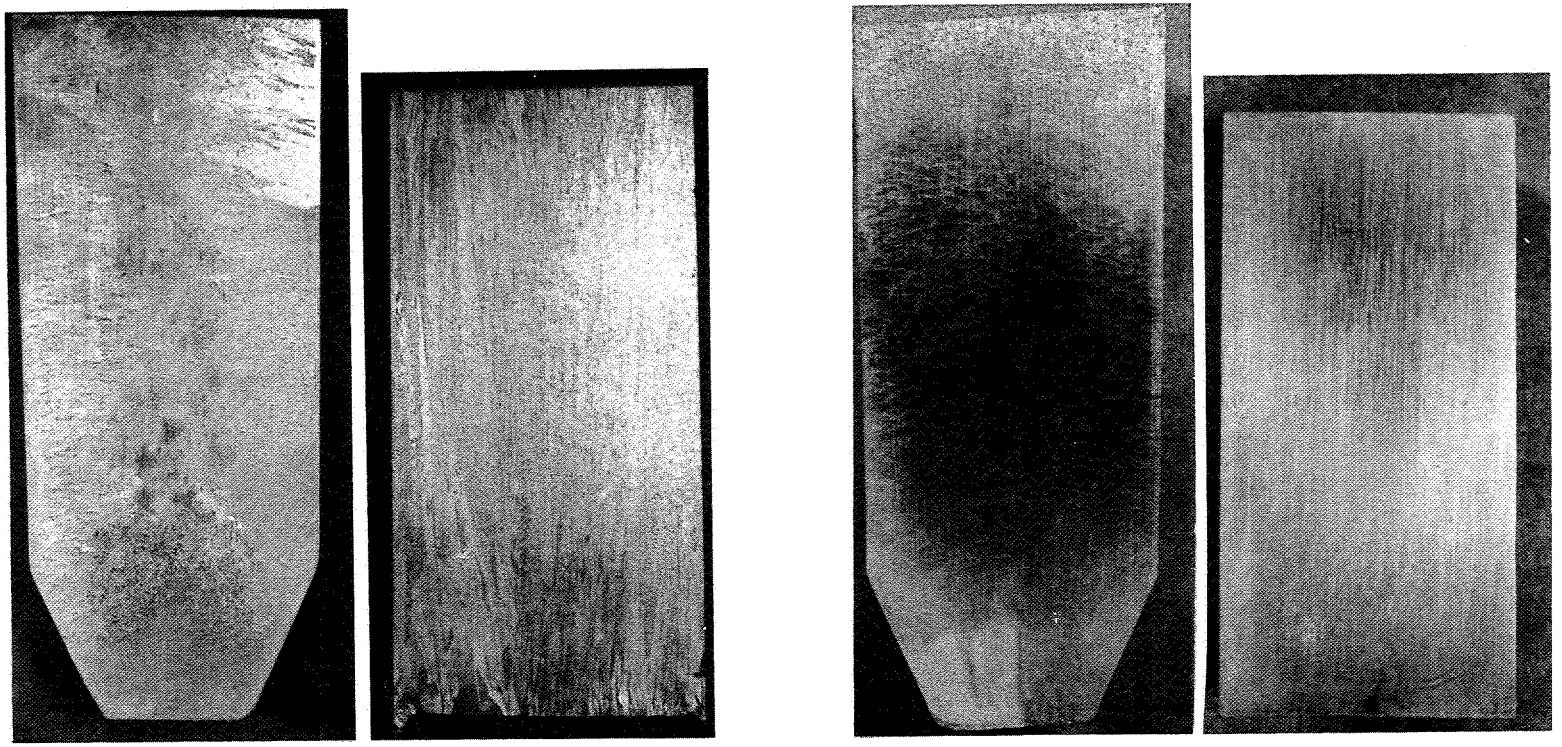

a) Co-35W-0.05Zr

b) Co-35W, 3Cr, 2Ti, 2Zr, 1C, 0.1B

Figure 20: Macrostructures of Conventionally Cast and Unidirectionally Solidified Ingots of Two Co-35W Base Alloys (etchant 2) Approximately 1X.

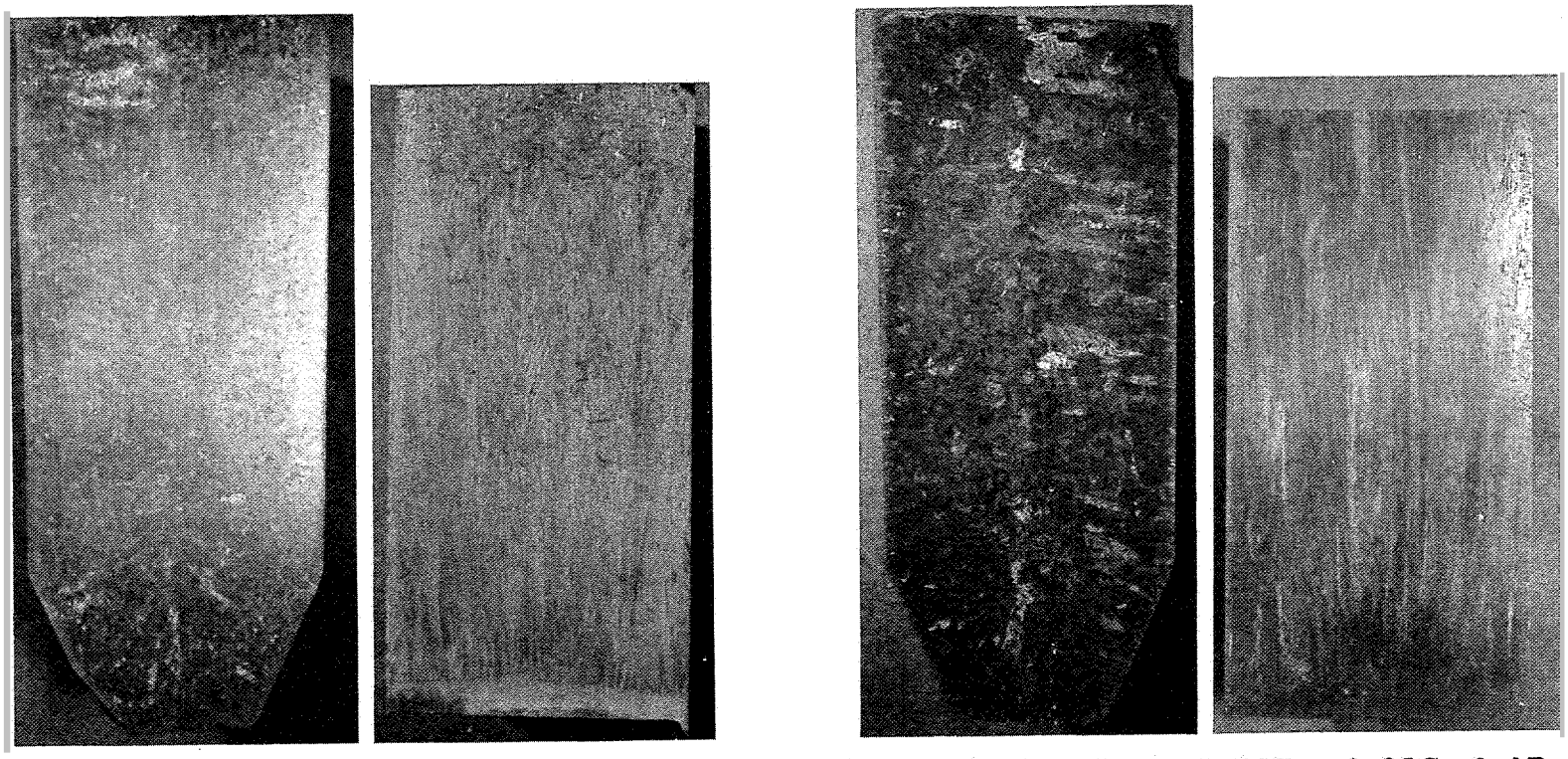

a) Co-45W-0.05Zr

b) Co-45W, 0.75Ti, 0.75Zr, 0.25C, 0.1B

Figure 21: Macrostructures of Conventionally Cast and Unidirectionally Solidified Ingots of Two Co-45W Base Alloys (Etchant 2) Approximately 1X.

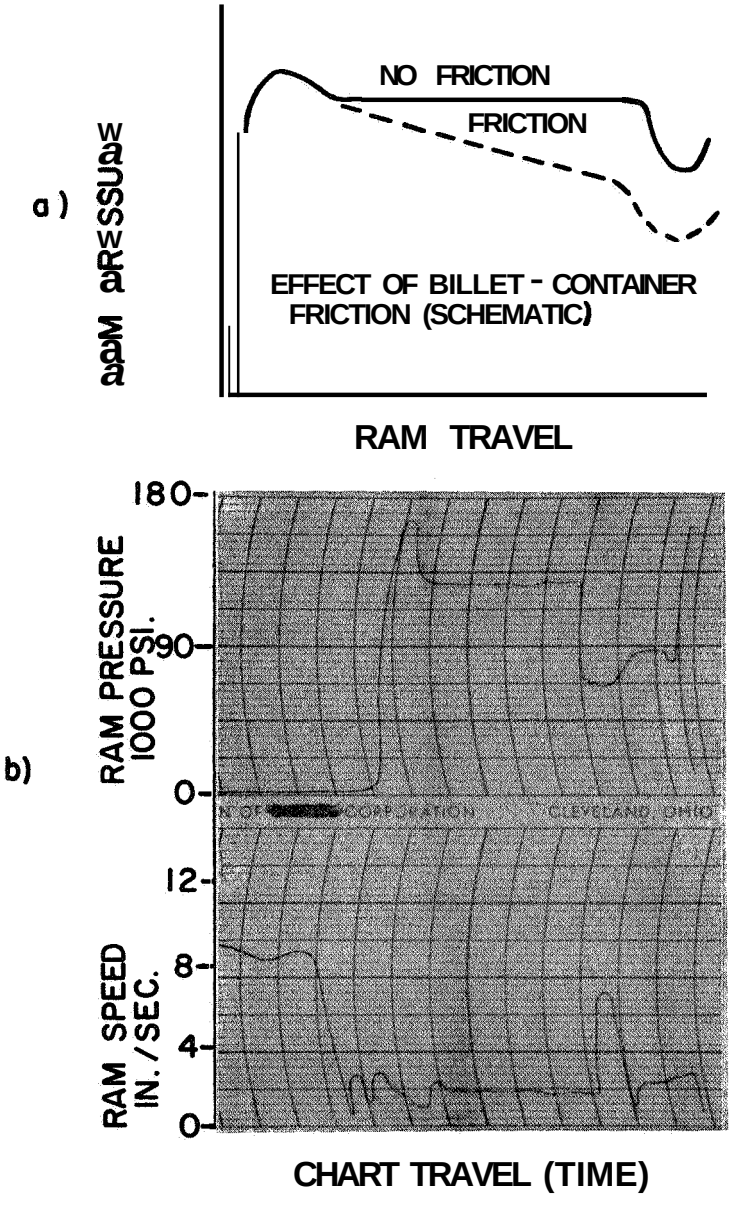

FIGURE 22: IDEALIZED EXTRUSION PRESSURE CURVE AND TYPICAL PRESSURE AND SPEED RECORD.

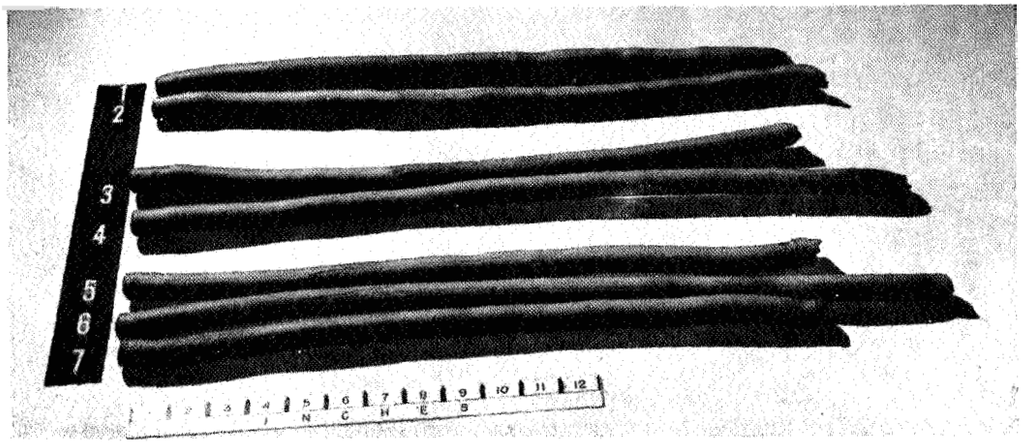

(a)

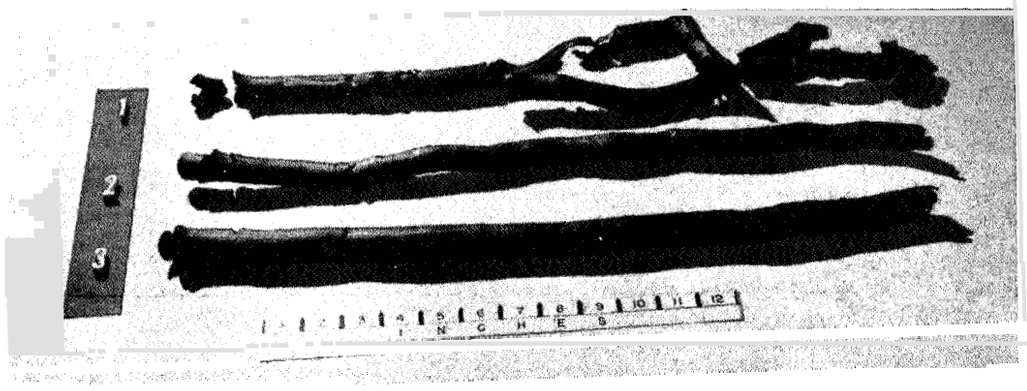

(b)

(a) 1, 2: Co-35W-0.05Zr
3, 4: Co-35W, 3Cr, 2Ti, 2Zr, 1C, 0.1B
5, 6, 7: Co-45W-0.05Zr

(b) 1, 2, 3: Co-45W, 0.75Ti, 0.75Zr, 0.25C, 0.1B

Figure 23: Appearance of As Extruded Bars.

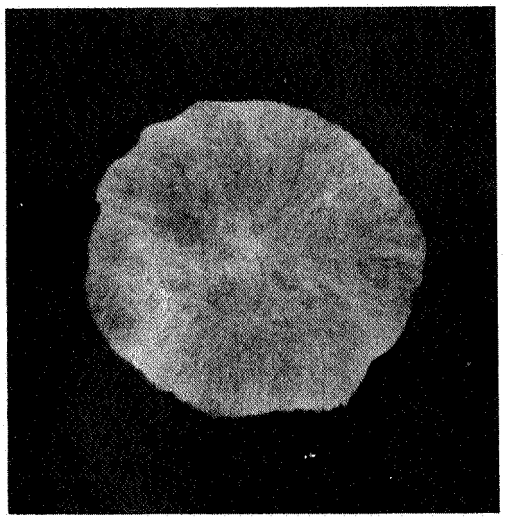

(a) Conventionally Cast

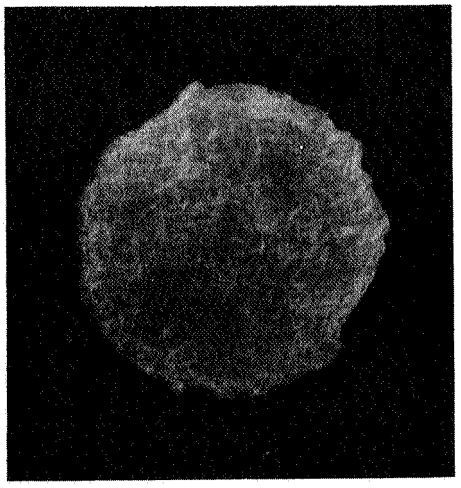

(b) Unidirectionally Solidified

Figure 24: Macrostructures of Extruded Co-35W-0.05 Illustrating Retention of Casting Ingot Pattern, (Etchant 2), Approximately 3 X.

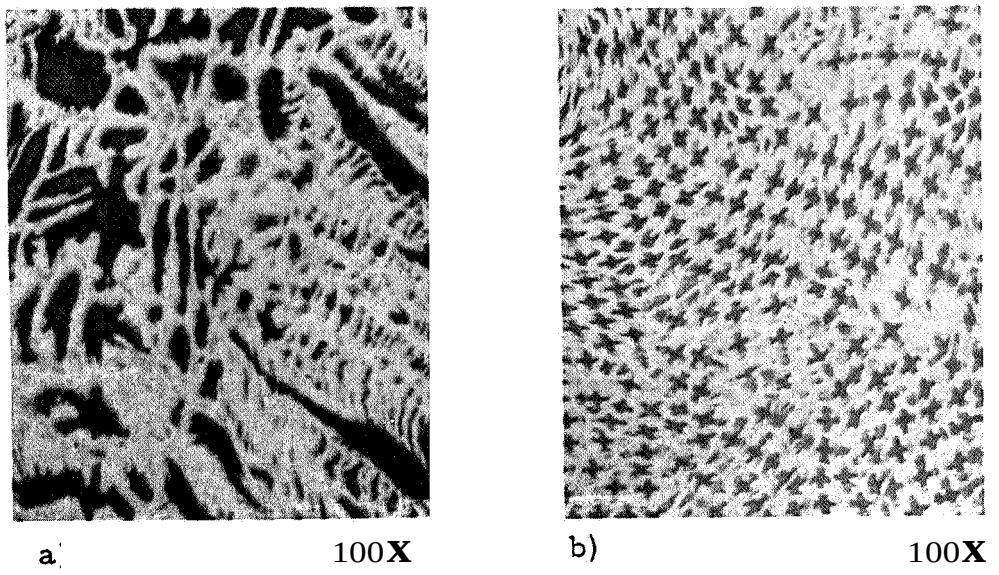

a) 100X b) 100X

Transverse (stain etch)

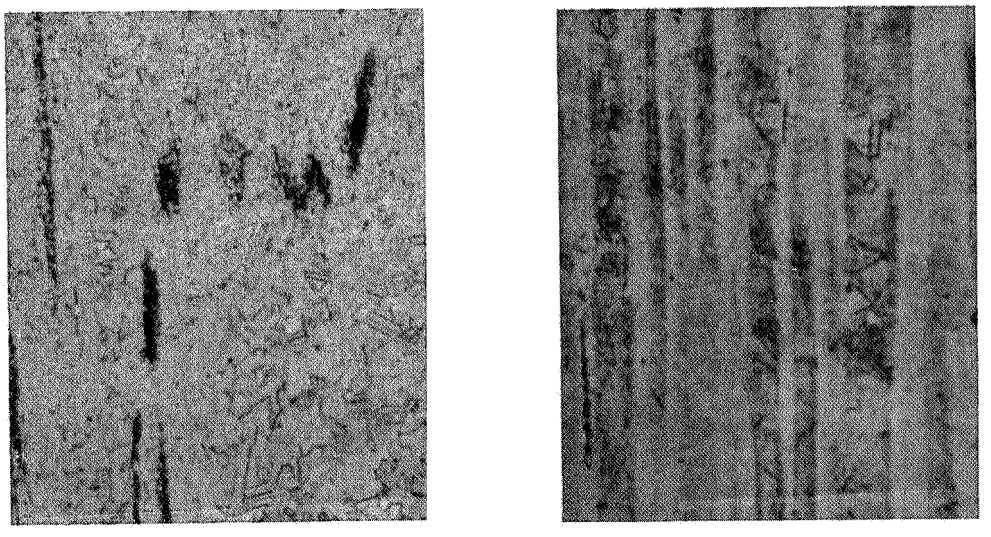

c) 250X d) 250X

Longitudinal

Figure 25: Microstructures of Extruded Co-35W-0.05Zr; (a,c) Conventionally Cast; (b,d) Unidirectionally Solidified (Etchant 1).

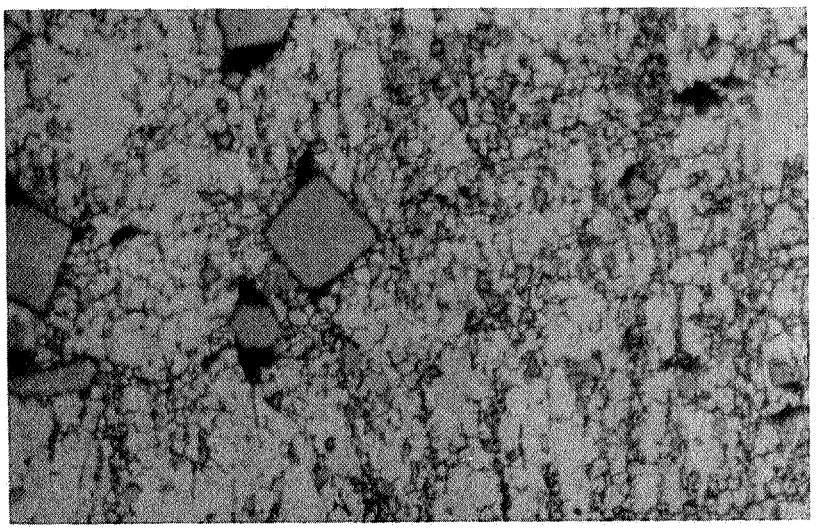

(a) 250X

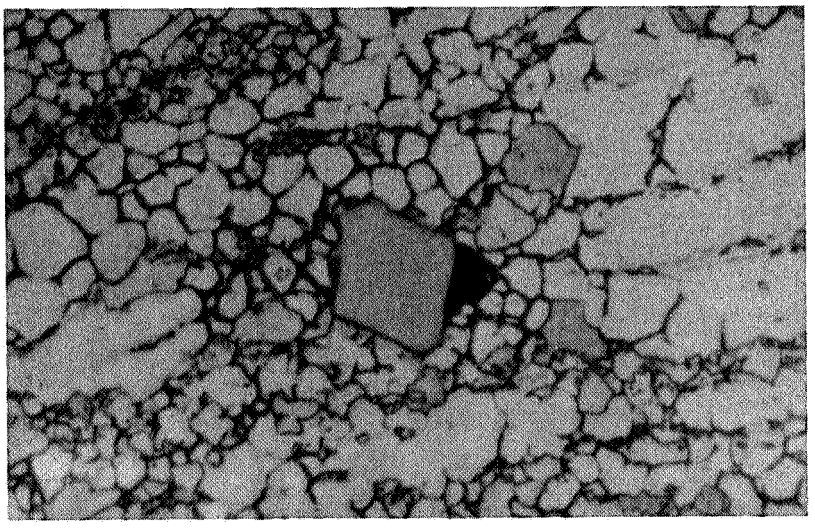

(b) 1000X

Figure 26: Microstructure of Extruded, Conventionally Cast Co-35W, 3Cr, 2Ti, 2Zr, 1C, 0.1B (Etchant 1).

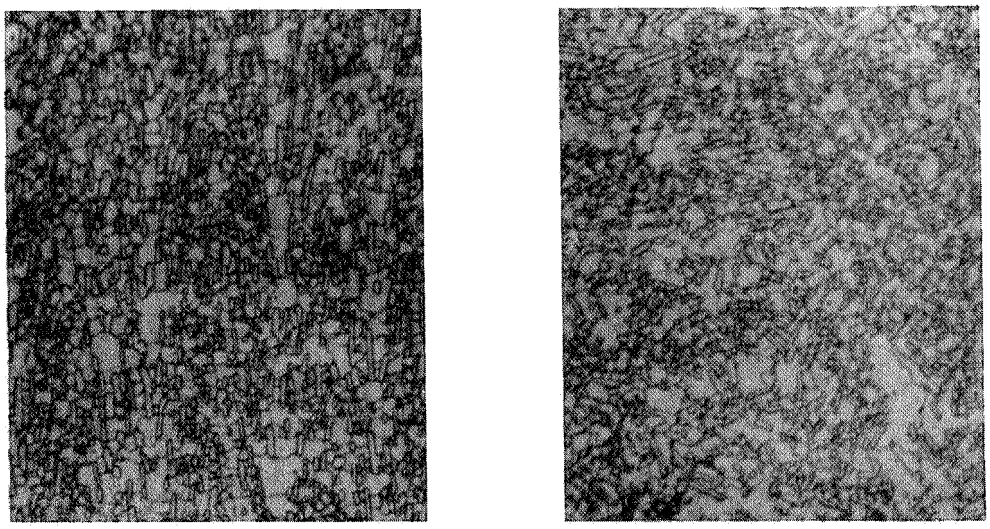

(a) (b)

Unidirectionally Solidified

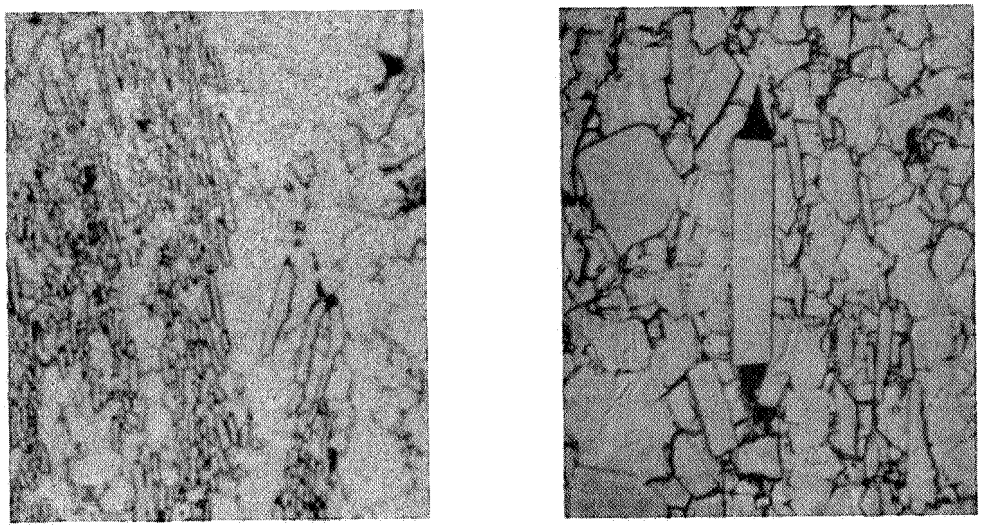

(c) (d)

Conventionally Solidified

Figure 27: Typical Extruded Structures of Co-45W-0.05Zr; (a, c, d) are Longitudinal Sections, (b) is Transverse, (Etchants 1 and 2), 1000X.

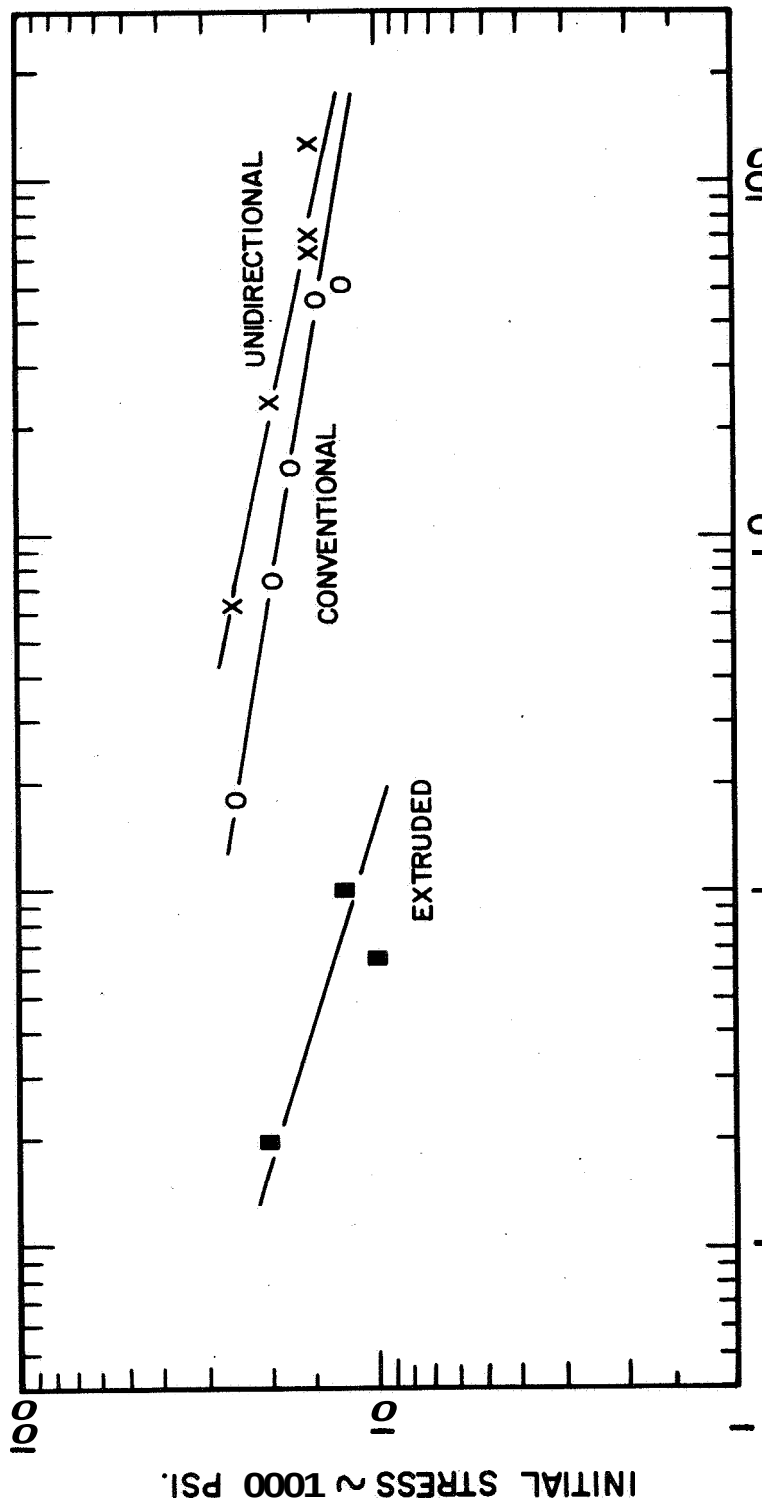

FIGURE 28: COMPARISON OF STRESS RUPTURE LIFE FOR AS CAST AND EXTRUDED Co-35 W, 0.05 Zr (TESTED IN AIR AT 1800°F).

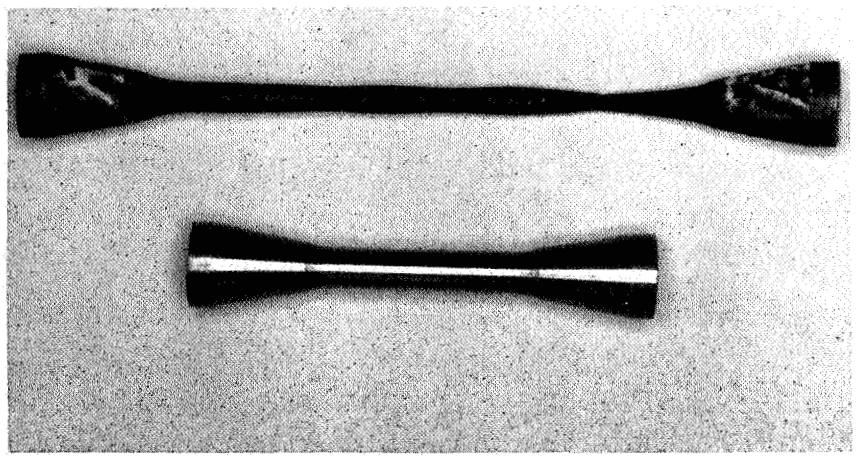

(a) Co-35W-0.05Zr, 174%Elongation, Multiple Necks

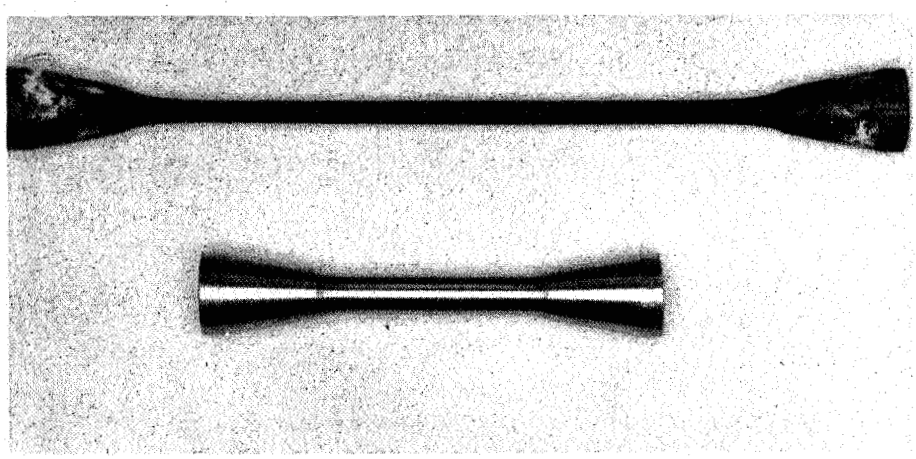

(b) Co-45W-0.05Zr, 212% Elongation, Without Fracture

Figure 29: Some Large Extensions Obtained in Stress Rupture Tests of Extruded Co-35W-0.05Zr and Co-45W-0.05Zr.

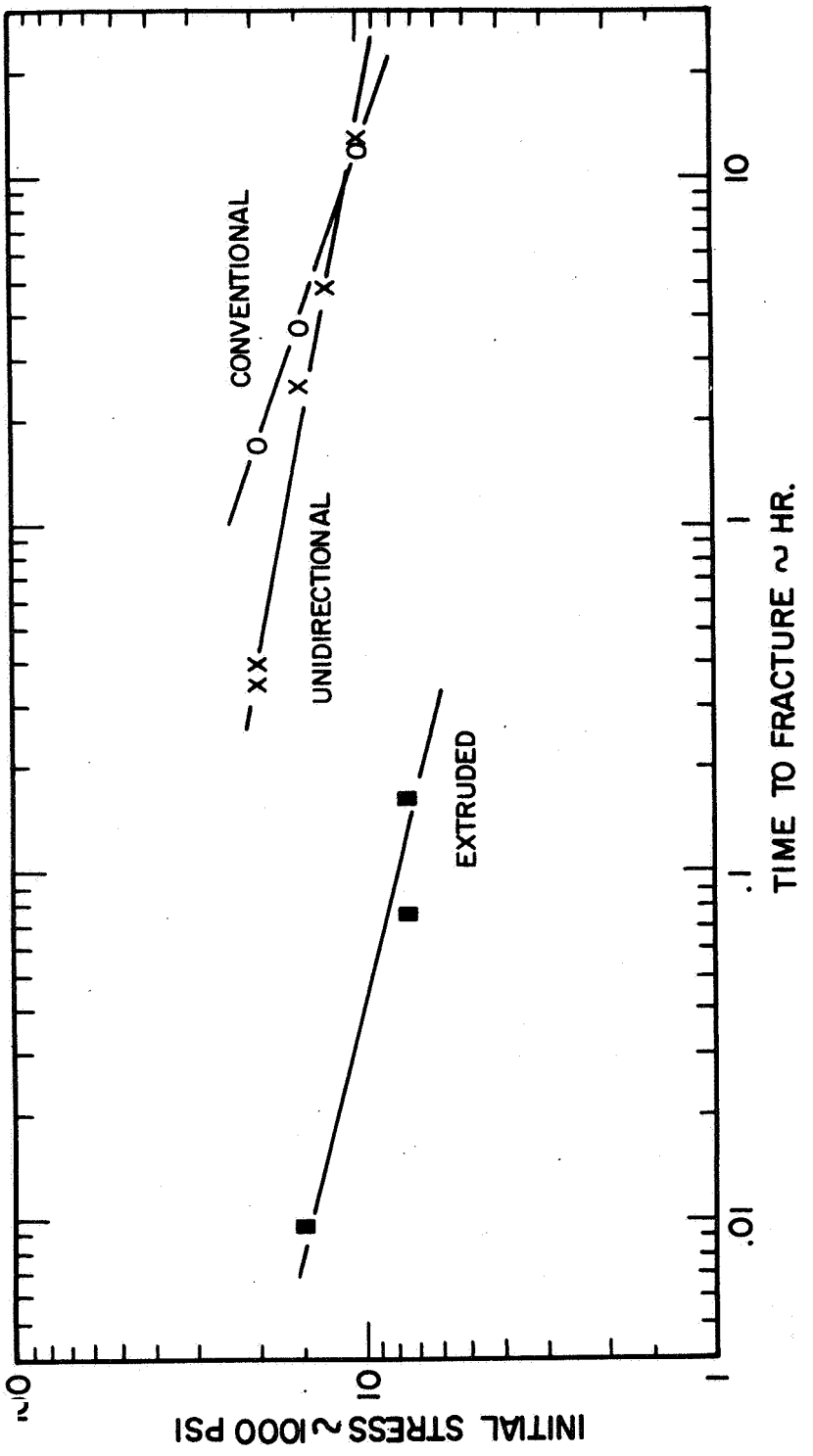

FIGURE 30: COMPARISON OF STRESS RUPTURE LIFE FOR AS CAST AND EXTRUDED Co – 45W, 0.05 Zr (TESTED IN AIR AT 1800°F).

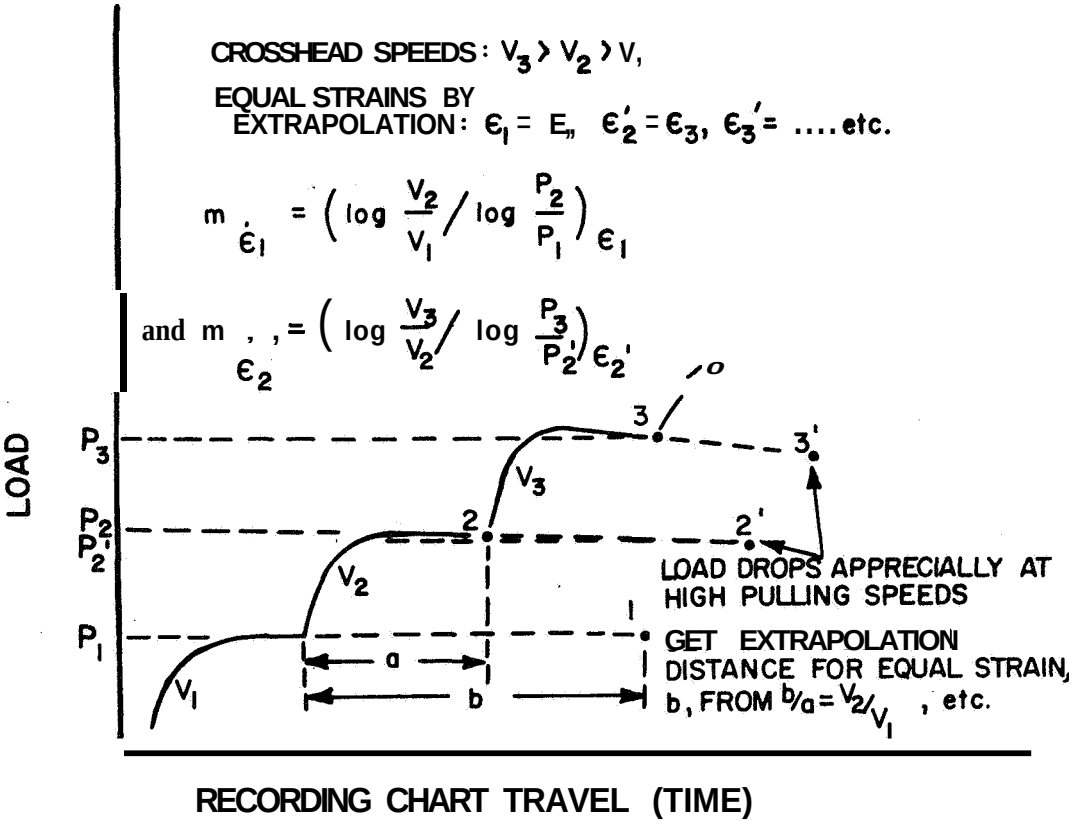

FIGURE 31: SCHEMATIC ILLUSTRATION OF DATA GENERATED IN TRANSIENT TENSILE TESTS AND CALCULATIONS OF STRAIN RATE SENSITIVITY INDEX, m.

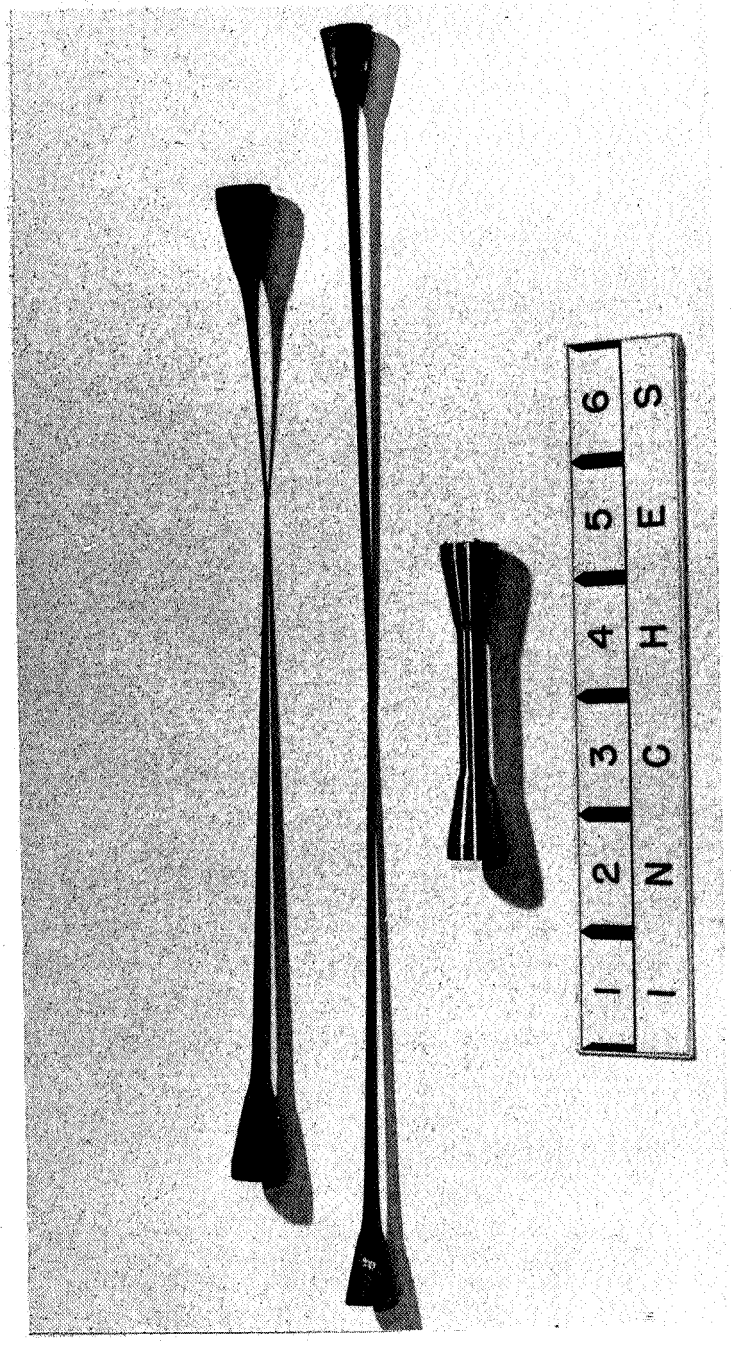

Figure 32: Examples of Large Elongations, 535 and 714%, Obtained in Hot Tensile Testing of Extruded Co-45W-0.05Zr.

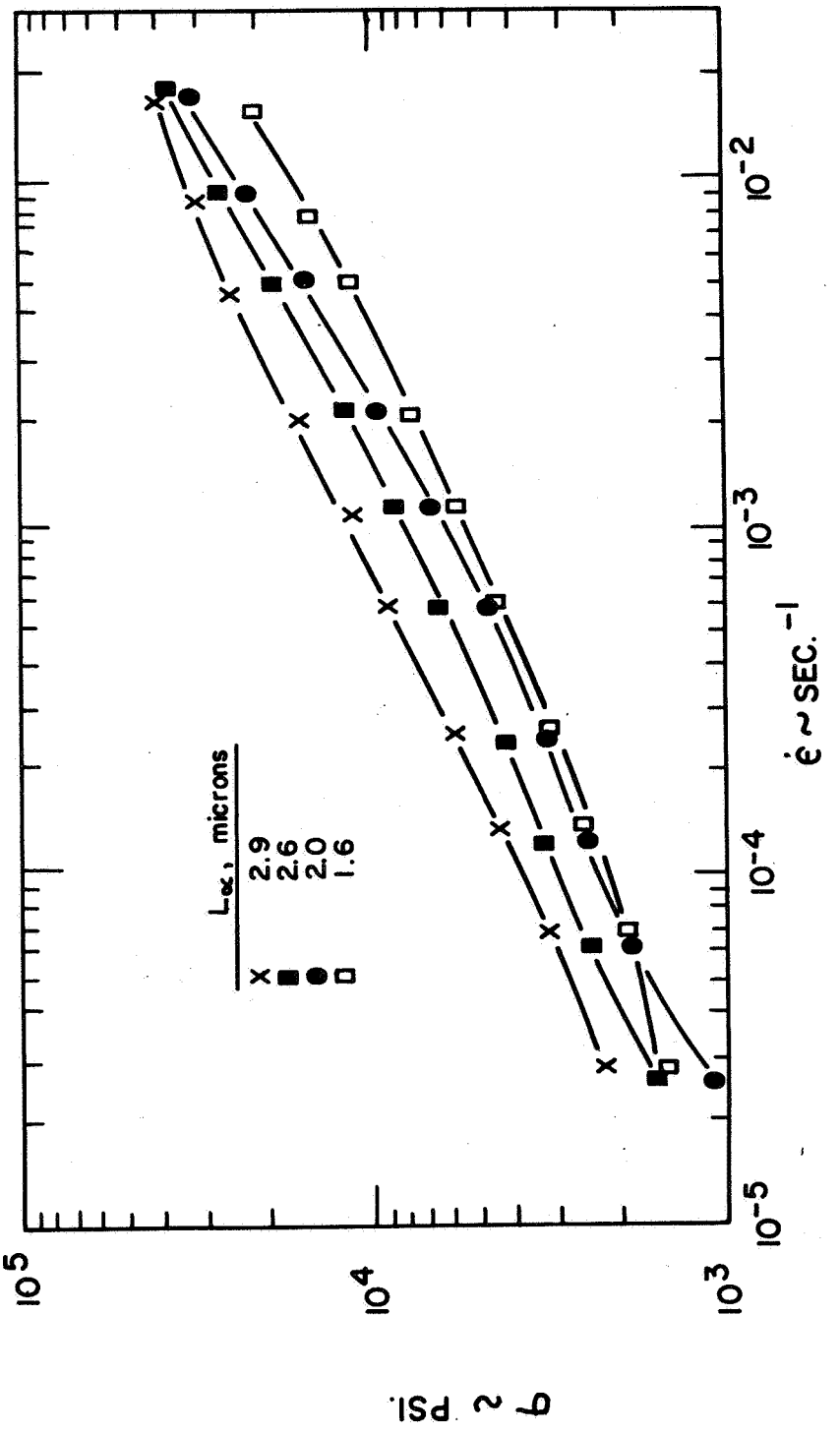

FIGURE 33: VARIATION OF FLOW STRESS, σ, WITH STRAIN RATE, $\dot{\epsilon}$, FOR EXTRUDED MATERIAL AT 1800°F.

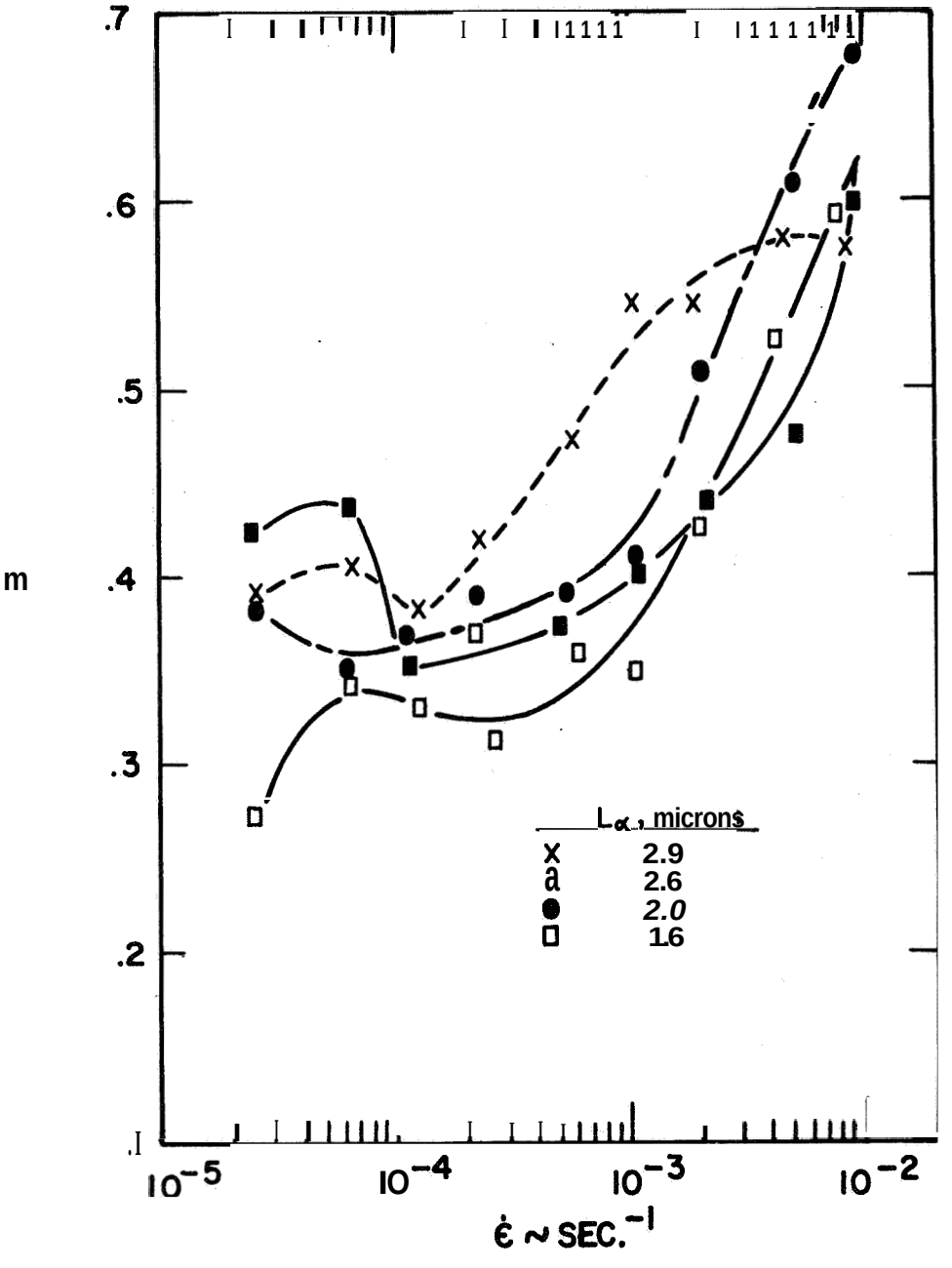

FIGURE 34: EFFECT OF STRAIN RATE ON THE STRAIN RATE SENSITIVITY INDEX, m, IN EXTRUDED MATERIAL AT 1800° F.

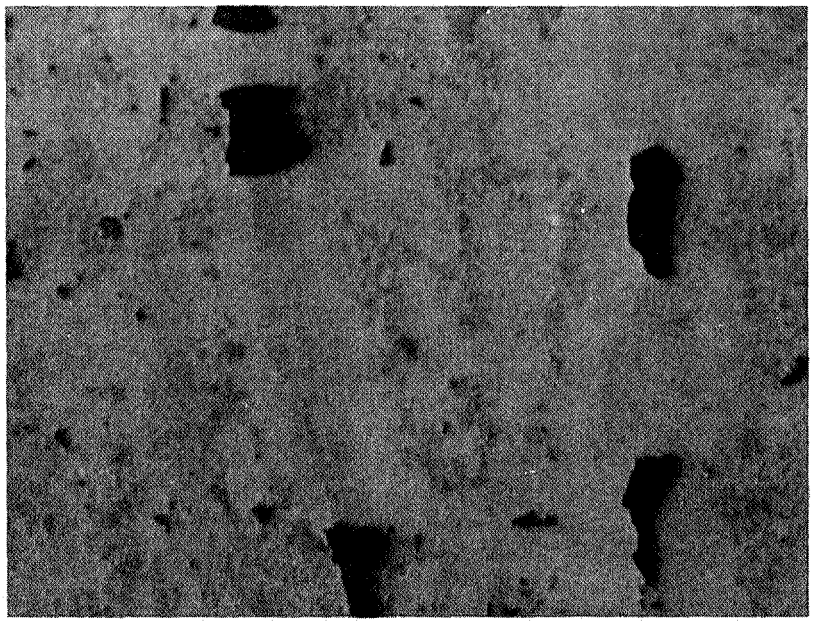

a) Etchants **1** and **2**

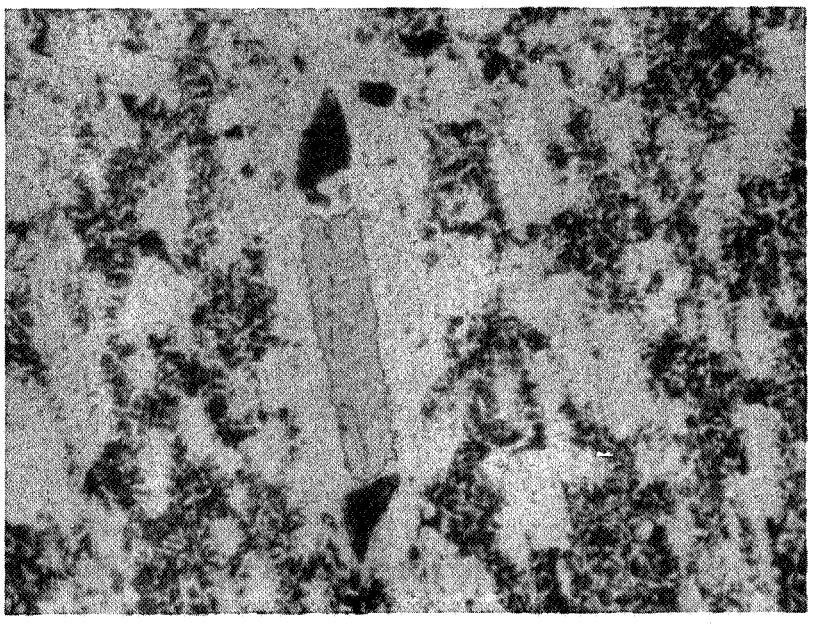

b) Etchants 3 **and 4**

Figure **35:** Partial Dissolution of W_6Co_7 and Precipitation in Extruded Co·45W-0.05Zr (Conventionally Cast) 1000**X.**

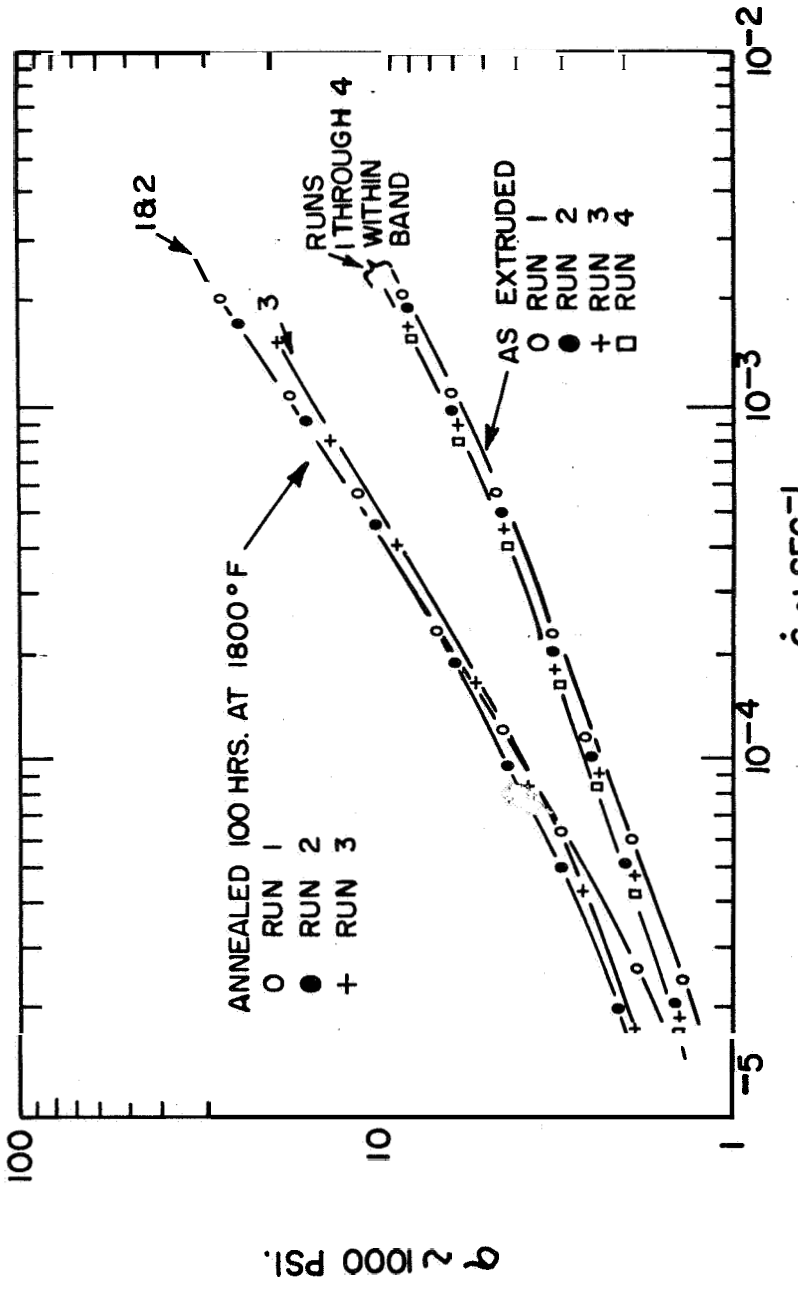

FIGURE 36: VARIATION OF FLOW STRESS, σ, WITH STRAIN RATE, $\dot{\epsilon}$, FOR AS EXTRUDED AND ANNEALED MATERIAL, (INITIAL, AS EXTRUDED GRAIN SIZE, L_α, ~ 1.8 AND 2.0 μ RESPECTIVELY.)

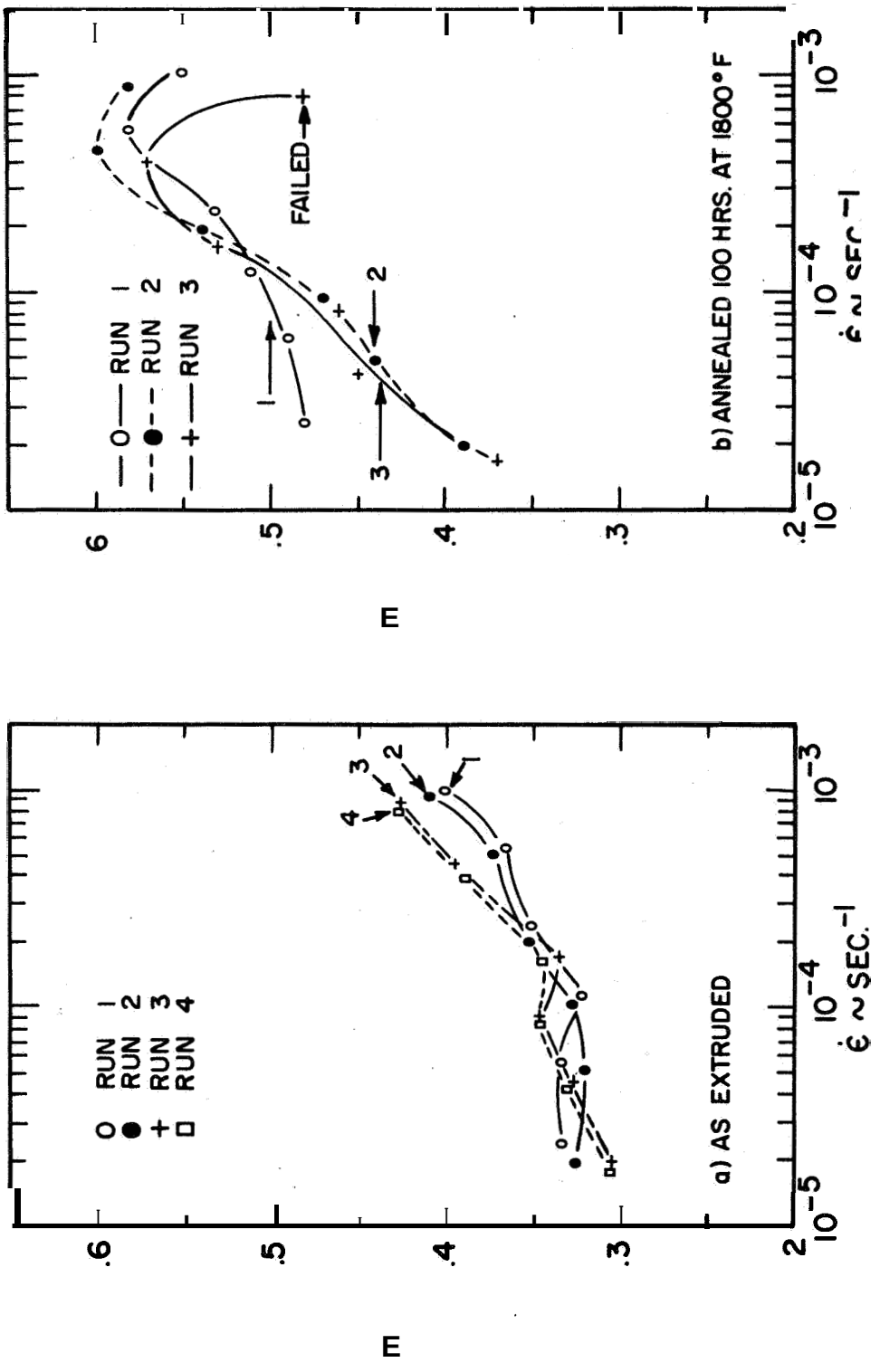

FIGURE 37. VARIATION OF STRAIN RATE SENSITIVITY INDEX, m, WITH STRAIN RATE, $\dot{\epsilon}$ FOR AS EXTRUDED AND ANNEALED MATERIAL (INITIAL AS EXTRUDED GRAIN SIZE, L_α ~ 1.8 AND 2.0 μ, RESPECTIVELY).

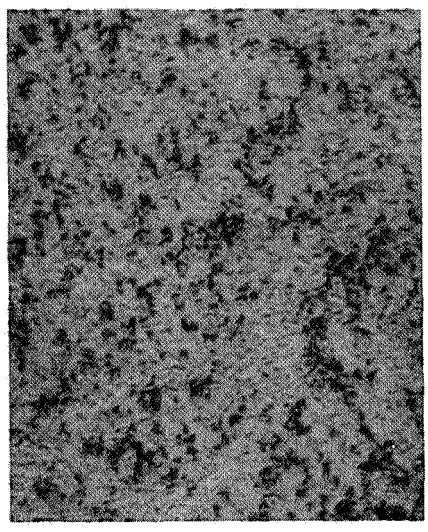

a) Grip 1000X

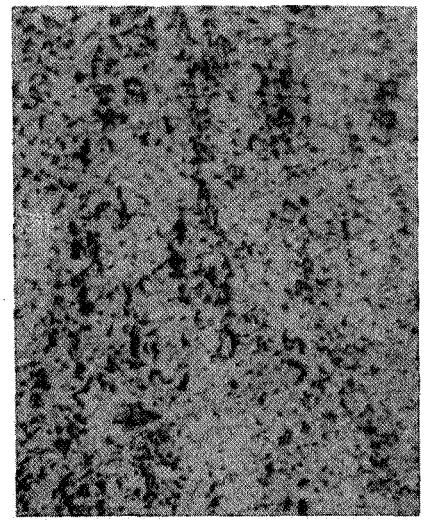

b) Test Section 1000X

a) Grip 2000X

b) Test Section 2000X

Figure 38: Structures Developed During Deformation of As Extruded Material; $L_\alpha \sim 1.8\ \mu$; Final Pulling Speed 2 in/min; Longitudinal Direction is Vertical in Photos (Etchants 3 and 4).

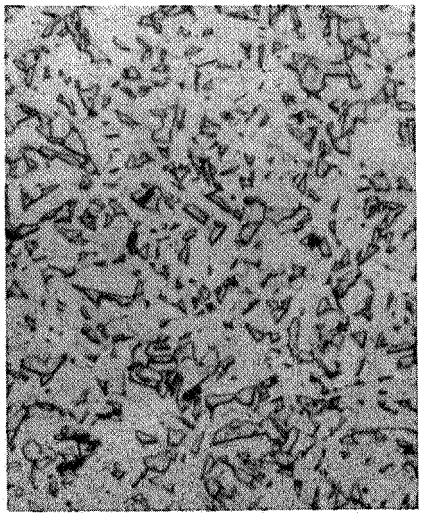

a) Grip 1000X

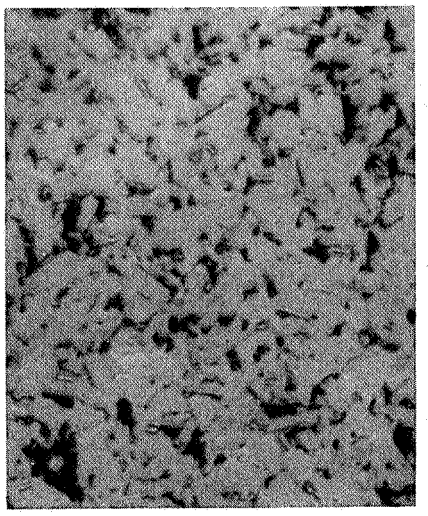

b) Test Section 1000X

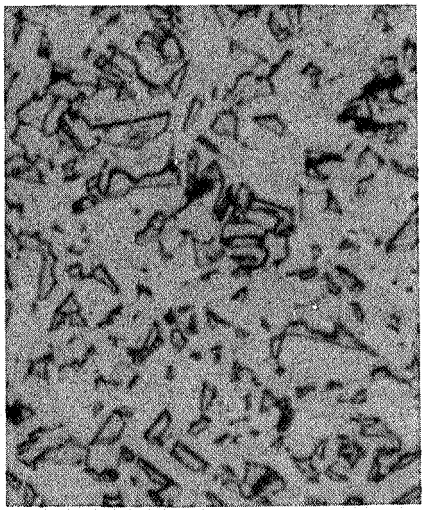

c) Grip 1500X

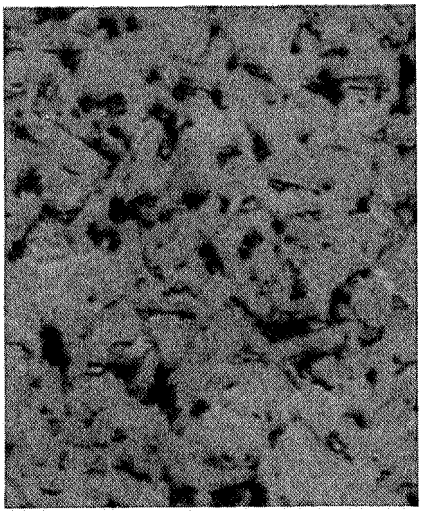

d) Test Section 1500X

Figure 39: Structures Developed During Deformation of Annealed Material; $L_\alpha \sim 2.0\mu$; Final Pulling Speed .2 in/min; Longitudinal Direction is Vertical in Photos (Etchants 3 and 4).